TE-19

# HYBRID DOPPLER-RADAR INERTIAL NAVIGATION TECHNIQUES FOR THE SUPERSONIC TRANSPORT AIRCRAFT

by

Frank Charles Sakran, Jr.

B. E. S., The Johns Hopkins University
(1960)

SUBMITTED IN PARTIAL FULFILLMENT
OF THE REQUIREMENTS FOR THE
DEGREE OF MASTER OF
SCIENCE
at the
MASSACHUSETTS INSTITUTE OF TECHNOLOGY
June 1967

Signature of Author Frank C. Sakran, Jr.
Department of Aeronautics and Astronautics, June 1967

Certified by W. Markey
Thesis Supervisor

Technical Supervisor

Accepted by
Chairman, Departmental Committee on Graduate Students

TE-19

# HYBRID DOPPLER-RADAR INERTIAL NAVIGATION TECHNIQUES FOR THE SUPERSONIC TRANSPORT AIRCRAFT

by

Frank Charles Sakran, Jr.

Submitted to the Department of Aeronautics and Astronautics on June 19, 1967 in partial fulfillment of the requirements for the degree of Master of Science.

## ABSTRACT

Two particular hybrid navigation systems utilizing both inertial and doppler radar sensors are studied for use in high speed aircraft such as the supersonic transport. The systems postulated consist of a semigeometric inertial system receiving linear velocity corrections from a Janus beam array doppler radar. System equations are linearized assuming constant aircraft velocity and quasistatic latitude. Response to constant component uncertainties of the two hybrid doppler-inertial systems is compared to that of a pure (undamped) inertial navigator. The predominant error sources are found to be either gyro drift or doppler radar bias propagating as a bounded oscillation in latitude and true heading, and unbounded in longitude.

Thesis Supervisor: Winston B. Markey, Sc. D.

Title: Professor of Aeronautics and Astronautics

## ACKNOWLEDGMENT

The author wishes to express his appreciation to his thesis advisor, Professor Winston S. Markey, and to Kenneth R. Britting, whose generous advice was very helpful in this effort.

Acknowledgment is also made to the MIT Computation Center for its work, done as Problem M5732.

This thesis was supported through NASA grant NGR 22-009-229 NASA Electronics Research Center, Cambridge, Mass., under Project DSR-70343.

TABLE OF CONTENTS

# CHAPTER I

# INTRODUCTION

The development of inertial and doppler radar sensors during the past two decades has enabled aircraft to obtain inflight navigational information without recourse to ground based equipment or restrictions incurred by weather or visibility. In some respects doppler radar and inertial techniques are competitive, and in some respects they are complementary. While both systems determine the aircraft's ground velocity vector, only the inertial system coordinatizes this vector in a navigational reference frame whose orientation is known with respect to the earth. The ground velocity vector obtained from the doppler radar is coordinatized in a frame fixed to the aircraft in which it is carried. To utilize doppler radar information for navigational purposes requires knowledge of the aircraft's heading. The resulting navigational information is thus limited in accuracy not only by the accuracy of the doppler radar, but also by that of the heading reference. Of the several sources of aircraft heading suitable for use in aircraft, an inertial system is the most accurate, and is not restricted by aircraft maneuvers, speed, or visibility.

An undesirable characteristic of inertial navigators is that imperfections in its mechanization result in errors which either grow unbounded with time or oscillate undamped with periods close to 84 minutes (the Schuler mode) and 24 hours (the earth rate mode) if the system is stationary on the earth. Not only are the system errors undesirable in themselves, but their oscillatory nature hinders effective application of real time position corrections derived from means external to the inertial navigator, such as radio, satellite, or celestial navigation aids. The inertial system would be more attractive if the oscillatory error modes could be damped. However damping by purely internal means invariably causes the system to exhibit errors as a function of vehicle motion; i.e., the system ceases to be dynamically exact. Such sensitivity to motion is particularly undesirable for a navigation system which is to be used in a high performance aircraft such as the supersonic transport, where both high accelerations and high rates of change of acceleration (jerk) would be encountered. If, however, some measure of vehicle velocity from a non-inertial source is available, the oscillatory modes may be

damped, with the system remaining dynamically exact. The doppler radar is such a source of vehicle velocity data.

Several systems combining inertial and doppler navigation systems have been produced for military aircraft applications. Only in the past several years have some aircraft in commercial service been equipped with either doppler or inertial systems. With the supersonic transport (SST) aircraft entering commercial service, the possibility of equipping the SST with both inertial and doppler radar sensors has been proposed as one solution to the needs of accurate navigation. The purpose of this analysis is to investigate two possible methods of combining inertial and doppler information for the SST application.

## CHAPTER II

## DOPPLER RADAR

### A. Principles of Doppler Radar

A doppler radar operates on the principle first described for sound waves by the Austrian physicist Christian Doppler in 1842; the frequency of waves detected by an observer is changed due to relative motion between the wave source and the observer. This frequency shift is observed not only for sound waves, but also for electromagnetic waves. The doppler navigation radar carries both transmitter (the electromagnetic wave source) and receiver (the observer) in the aircraft, and compares the frequency of transmitted and received energy (Fig. 1). Here the doppler frequency shift is due to the component of relative velocity between the aircraft and the discrete objects on the surface overflown which are illuminated by the beam and which backscatter energy in the direction of the receiver.

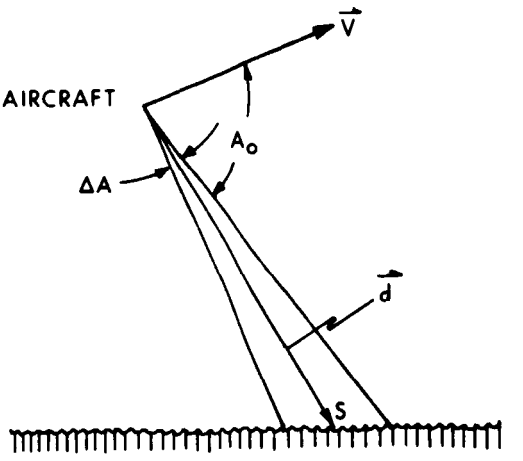


Fig. 1 Geometry of Single Beam Doppler Radar

When the relative velocity between source and observer is small compared to that of the energy through the propagation medium, the following derivation of the expression for the observed doppler frequency shift is valid (a rigorous derivation including relativistic effects is given by reference (1) ). The transmitted energy may be represented as $E_t = a \sin 2\pi f_t t$ and the energy at the receiver from scattering particle S as $E_r = b \sin (2\pi f_t t - \phi)$, where a and b are dependent upon equipment characteristics,absorbtion by the propagation medium, and the radar reflectivity of the scatterer S. The phase lag $\phi$ is due to the propagation delay time (round trip path) : $\phi = 2\pi \frac{2d}{\lambda}$, where $\vec{d}$ is the position vector from the aircraft to scatterer S, and $\lambda$ is the wavelength of the transmitted microwave energy. Since the aircraft is moving relative to S, d and hence $\phi$ is time varying. For short intervals of time and aircraft velocities relative to S that are small compared with the speed of propagation of the microwave energy ($3 \times 10^8$ meters/second), $d(t) = d_o - \frac{\vec{V} \cdot \vec{d}}{d} t$, where $d_o$ is the value of d at $t = 0$. Substituting, $E_r = b \sin\left[2\pi f_t t - \frac{4\pi}{\lambda}(d_0 - \frac{\vec{V} \cdot \vec{d}}{d} t)\right] = b \sin \left[(2\pi f_t + \frac{4\pi \vec{V} \cdot \vec{d}}{\lambda} t - \phi_o\right]$ where $\phi_o = \frac{4\pi d_o}{\lambda}$ is a fixed phase lag. Comparing the frequencies of transmitted and received energies, $f_{DOP} \triangleq f_r - f_t = \frac{2 \vec{V} \cdot \vec{d}}{\lambda d}$. Since $\frac{\vec{V} \cdot \vec{d}}{d}$ is the component of $\vec{V}$ in the direction of $\vec{d}$, measurement of $f_{DOP}$ with a beam in any direction (so long as it illuminates a scattering surface) enables determination of the component of $\vec{V}$ in that direction. A minimum of three non-coplanar beams is necessary to completely determine the aircraft's velocity vector.

B. Doppler Velocity Coordinate Resolution

Although doppler radars are able to sense the aircraft's total velocity vector (with respect to the scattering surface overflown), this vector as sensed is coordinatized in a frame fixed to the radar's antenna structure. To be compatible with the inertial system the doppler velocity vector must be transformed to navigational coordinates. This is accomplished in two steps: reduction of the radar-sensed velocity to the two components lying in the local horizontal plane, and then resolution about true heading angle to yield true north and east components. The airframe attitude and true heading angles necessary to effect this resolution may be measured by using the controlled member of the space integrator in a semi-geometric system.

The method by which the horizontal components of velocity are derived from doppler information are first investigated. Most of the current generation of doppler radars use a Janus beaming technique, named after the Greek god who looked forward and backward. Here a component of the aircraft's velocity with respect to the surface overflown is sensed by a pair of beams as in Figure 2.

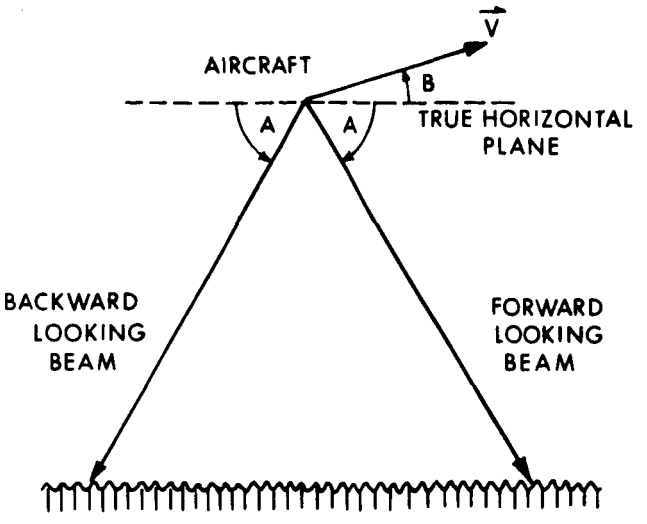


Fig. 2 Geometry of Janus Beam Pair

The frequency of the received energy of the backward-looking beam is $f_{r_1} = f_t - \frac{2V}{\lambda} \cos (A - B)$, and that of the forward-looking beam is $f_{r_2} = f_t + \frac{2V}{\lambda} \cos (A + B)$. A is the depression angle of the beams below the local horizontal plane, and B is the climb angle of the aircraft (the angle between the velocity vector V and the local horizontal plane). The signal of interest is not $f_r - f_t$ as before, but the difference between the two received frequencies $f_{r_2} - f_{r_1}$:

$$f_{r_2} - f_{r_1} = \frac{2V}{\lambda} \left[\cos (A + B) + \cos (A - B)\right] = \frac{4V}{\lambda} \cos A \cos B$$

The component of aircraft's groundspeed in the plane of the two beams, which is defined as V cos B, is then determined as $V \cos B = \frac{\lambda}{4 \cos A} \left(f_{r_2} - f_{r_1}\right)$. The angle A is the depression angle of each beam below the horizontal plane, and is the sum of the angle between the beams and the airframe and the attitude angle between the airframe and the local horizontal plane, each measured in the plane of the beams. The airframe attitude angle is established by means external to the doppler radar; say an inertial system. Consider this airframe attitude angle to be in error by $\delta A$. Then

$$f_{r_2} - f_{r_1} = \frac{2V}{\lambda} \left[\cos(A - \delta A + B) + \cos(A + \delta A - B)\right] = \frac{4V}{\lambda} \cos A \cos (\delta A - B)$$

from which is solved $V \cos (B - \delta A) = \frac{\lambda}{4 \cos A} \left( f_{r_2} - f_{r_1} \right)$.

The relative error in the computed groundspeed component is then

$$\frac{\cos (B - \delta A) - \cos B}{\cos B} = \cos \delta A + \sin \delta A \tan B - 1 \cong \delta A \tan B \text{ for small } \delta A.$$

Thus for small climb angles, as in steady flight, reasonable inaccuracies in airframe attitude information result in negligibly small errors in doppler-derived groundspeed. For this reason, coupling of the inertial platform's vertical correction angles into doppler groundspeed information may be neglected. There remains the resolution of the horizontal components of aircraft velocity into navigational coordinates, i.e., true north and east. Again, the necessary angular information (airframe true heading) is supplied by the inertial system.

C. Doppler Noise Content

The above discussion assumed that the microwave energy is emitted as rays with zero beamwidth. In actuality, with transmitter antennas of practical size for airborn use, the emitted beams are at least several degrees wide. Since the received energy is now backscattered from a range of A angles, the doppler difference signal $f_{DOP}$ is not a single frequency but a continuous spectrum. The half-power width of the mean doppler spectrum is $\Delta f_{DOP} = \frac{2V}{\lambda} \Delta A \sin A_o$, where $A_o$ and $\Delta A$ are defined as in Figure 1. The spectrum is not constant with time at any velocity, since individual scatterers on the overflown surface vary in radar reflectivity. It is the task of the doppler frequency tracker to determine the center of power of the doppler spectrum corresponding to the component of aircraft groundspeed in the plane of the beams. If the tracker is sufficiently fast to chase the fluctuation noise caused by the various discrete scatterers as they pass through the beam, this fluctuation noise shows up in the radar's velocity determination as an added noise signal. The alternative, slowing down the response of the tracker to reduce noise, has the undesirable effect of making the tracker insensitive to actual high-frequency changes in aircraft velocity. Thus doppler radars may be characterized as having good low-frequency aircraft velocity tracking ability but poor response to high-frequency changes in velocity, along with a high noise content. This is an contrast to the inertial system, which exhibits good high-frequency response but in which the predominant errors are of low (Schuler) frequency.

# CHAPTER III

## HYBRID INERTIAL-DOPPLER SYSTEMS

It would appear beneficial to somehow combine the doppler radar's low-frequency response with the inertial system's high-frequency response. This could be accomplished simply by mixing the two independent velocities in a suitable filter, and the resultant hybrid velocity signal integrated to obtain present position. In this case the inertial system's space integrator angular errors would continue to oscillate undamped. To damp these angular errors, the doppler velocity must be introduced internal to the inertial system's Schuler loops. Damping the angular errors is desirable since doppler radar outputs are sometimes unavailable during portions of flight. One not infrequent cause of doppler loss is flight over slick water surfaces, wherein insufficient energy is backscattered toward the receiver for reliable doppler frequency tracking. Doppler radars transmit in one of two assigned frequency bands centered at 8.8 gHz and 13.3 gHz, corresponding to wavelengths of 3.4 cm and 2.3 cm respectively. If the overflown water surface is not broken by wavelets of length smaller than the wavelength of incident radar energy, little energy will be backscattered to reach the receiver. Flight at high altitudes further decreases received energy. During periods of doppler loss the navigation system reverts to pure undamped Schuler tuned inertial operation. Were the platform error angles undamped, the navigational data would be subject to increased error during periods of doppler loss.

### A. Single-Axis Inertial-Doppler Systems

Figure 3 shows a general mechanization for damping the oscillations of a single-axis inertial system. The gains $H_1$, $H_2$, and $H_3$ may be functions of frequency. Figure 4 is the corresponding signal flow diagram where the system is taken to be stationary on a spherical nonrotating earth. The characteristic equation of this single-axis system is

$$p^2 + \frac{H_1(p)}{1 + H_3(p)}p + \left(\frac{1 + H_2(p) + H_3(p)}{1 + H_3(p)}\right)\frac{g}{R} = 0.$$

In contrast to a pure inertial system $\left(H_1(p) = H_2(p) = H_3(p) = 0\right)$ which oscillates

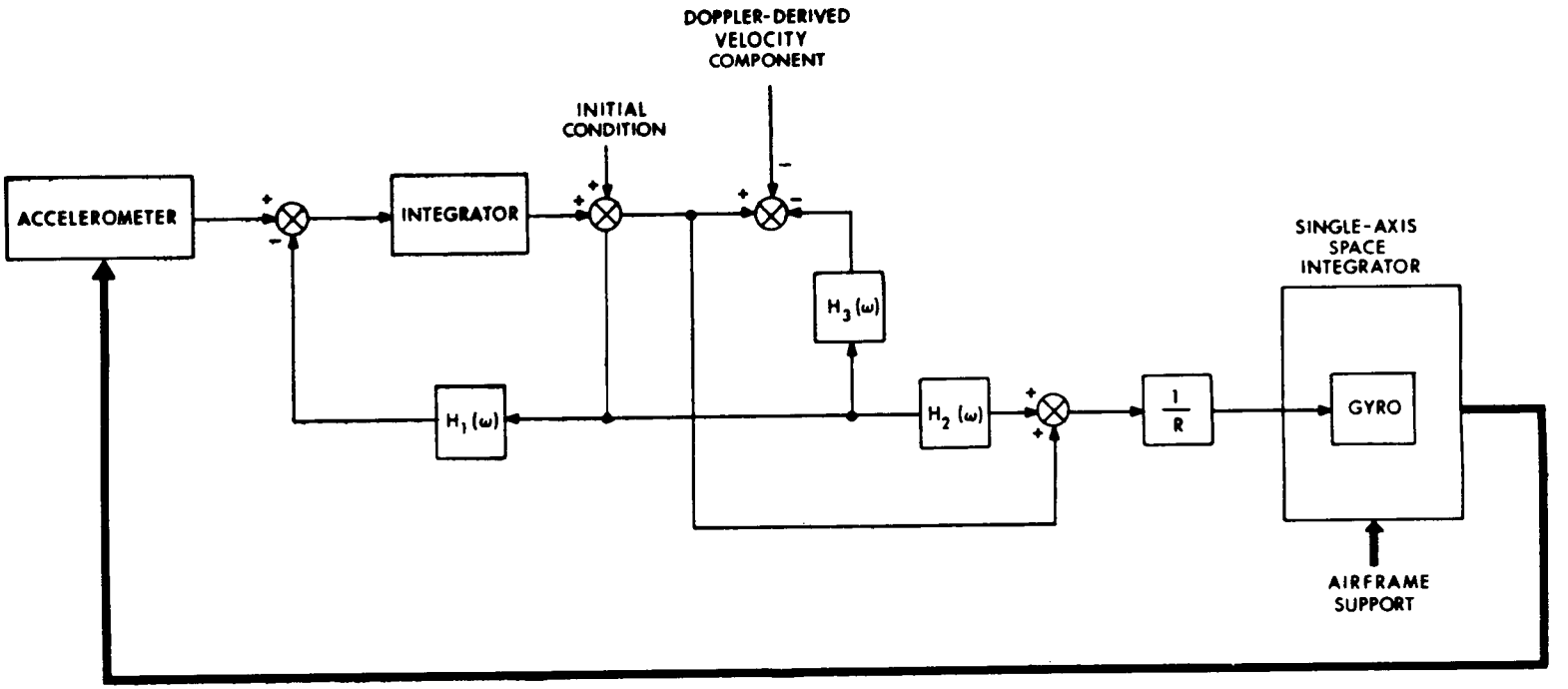


Fig. 3 Mechanization of a Single-Axis Inertial-Doppler Navigator

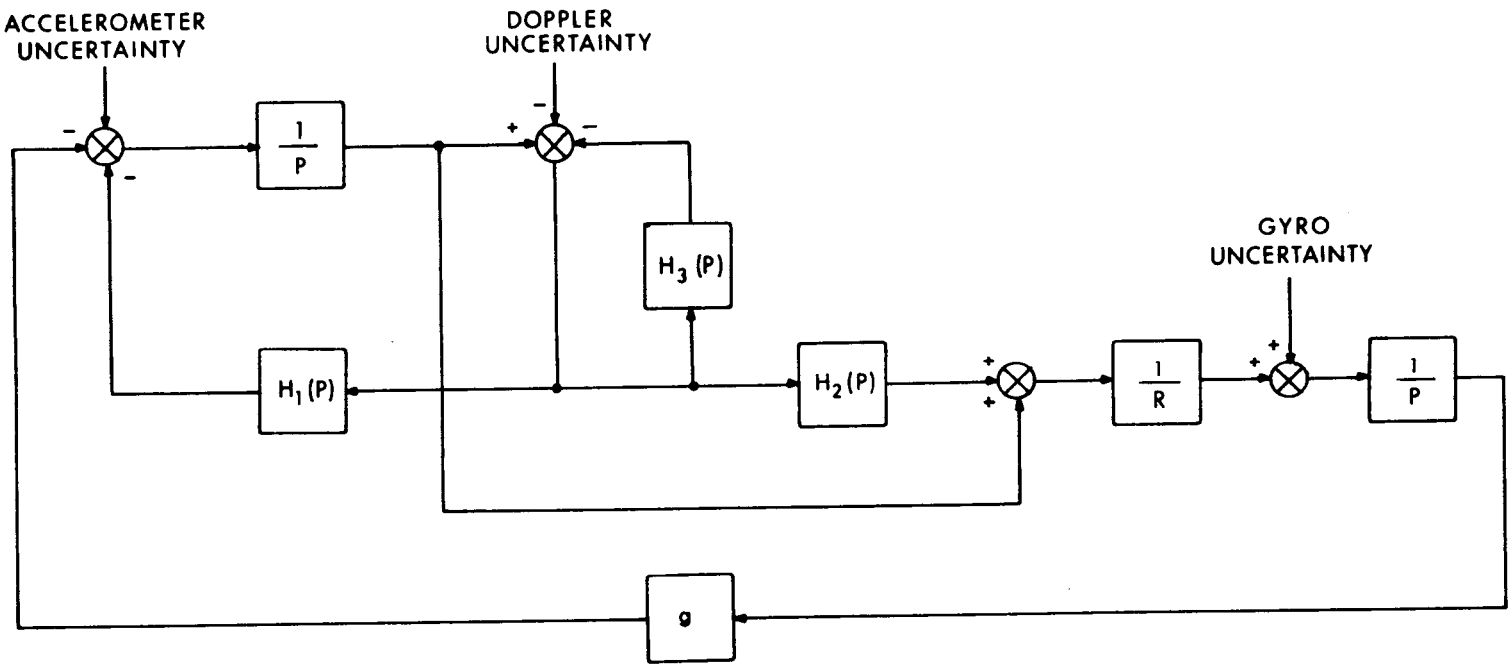


Fig. 4 Signal Flow Diagram of Single-Axis Inertial-Doppler Navigator Stationary on Spherical Non-Rotating Earth

undamped with natural frequency $\omega_s = \sqrt{\frac{g}{R}}$, the doppler-aided system's natural frequency may be raised at will, and be damped. Arbitrarily short solution times may then be achieved. The penalty of raising the system's natural frequency is an increased sensitivity to the high-frequency noise in inertial and doppler sensor outputs. Doppler fluctuation noise in particular can be an important source of system error. The functions $H_2(p)$ and $H_3(p)$ may include pure integrators serving to cancel either gyro or doppler constant bias uncertainties. The exact form of navigational errors depends on the point in the Schuler loop at which navigational information is extracted. Infinitely many combinations of outputs and choices of functions are possible. References (2)-(5) discuss some of the possible configurations in detail. W. A. Porter, in reference (6), develops a general approach to the synthesis of this type of system.

All of the available literature appears to be based on such a single-axis approach wherein the system is assumed stationary on a nonrotating earth. This has the advantage that the resulting error transfer functions are relatively simple. System design may then proceed by determination of the H(p) functions based on some a priori definition of system optimization. There are however two mechanisms that affect system performance that are implicitly excluded in a single-channel analysis. Their importance depends on the nature of the mission flown by the aircraft carrying the navigation system.

(a) Broxmeyer in reference (7) has shown the existence of a "space rate" oscillatory mode in a pure inertial navigator which is created by the interdependency of computed gyro space rate commands and computed latitude. For a system stationary on the rotating earth, this leads to an oscillatory mode with a 24 hour period. Aircraft easterly velocity decreases this period. At SST speeds, crossing the Atlantic from west to east, say from New York to London, will require inertial system operation for over one-half of the space rate mode period. Clearly, the influence of this mode on navigational errors is of interest in SST applications.

(b) As previously noted, the doppler radar determines ground velocity components in airframe coordinates. Before injection into the inertial Schuler loops, doppler ground velocity ideally should be transformed into navigational frame coordinates. Since in actuality the inertial system is utilized for this purpose, error in the space integrator's true heading angle will generate errors in the doppler velocity components. As aircraft speed increases, the magnitude of these cross-coupling errors in doppler velocity increase. Since the platform heading angle error varies with time, the doppler velocity cross-coupling terms can affect the dynamics of the combined system.

B. Three-Axis Inertial-Doppler System Analysis

The above considerations suggest that the usual stationary single-axis approach to inertial-doppler navigation system design may not be adequate for high speed aircraft such as the SST. A three-axis analysis was therefore undertaken. The inertial configuration chosen is a semi-geometric system wherein the accelerometers are mounted along the level axes of the controlled member of a space integrator which is commanded such that its axes are ideally always coincident with those of the local navigational frame. The doppler radar is assumed to utilize a Janus beam configuration, so that the only coupling of signals from inertial system to doppler radar is through the inertial true heading angle. Doppler to inertial coupling is by two constant gains in each Schuler loop. Referring to figure 3, $H_1(\omega) = \gamma$, and $H_2(\omega) = \alpha$. $\gamma > 0$, $\alpha \geq 0$, and both $\gamma$ and $\alpha$ are independent of frequency. The mechanization of the complete system is shown in Figure 5. It is not claimed that this particular form of combined system is best for the SST application. It was chosen only because it represents the type of hybrid system now operational in many military aircraft.

Several approximations were made in order to simplify the analysis and to allow the application of linear transform techniques. The approximations are:

(a) The earth is assumed to be rotating at constant angular velocity and to be spherical with radius R. The assumption of a spherical earth is not valid in the mechanization of an actual system, but does not appreciably affect results of an error analysis, as shown in reference (8).

(b) The coriolis terms necessary to correct the accelerometer outputs in order to obtain northerly and easterly accelerations are assumed to be perfectly computed and applied, thus exactly cancelling the physical coriolis components sensed by the accelerometers.

(c) The initial space integrator controlled member misalignment correction angles are small, so that the usual small angle approximations $\sin C(0) \cong C(0)$ and $\cos C(0) \cong 1$ are valid. The instrument uncertainties are sufficiently small that the control member correction angles and the computed latitude correction angle remain small throughout system operation. Also, products of uncertainites and correction angles are neglected.

(d) The aircraft is assumed to be flying with constant northerly and easterly velocity components.

(e) Quasi-static operation is assumed in the north direction; i.e., northerly velocity is admitted, but the aircraft's latitude and trigonometric functions of latitude are treated as constants. The latitude computed by the system is considered to be the sum of a constant (correct) value and a time-varying error.

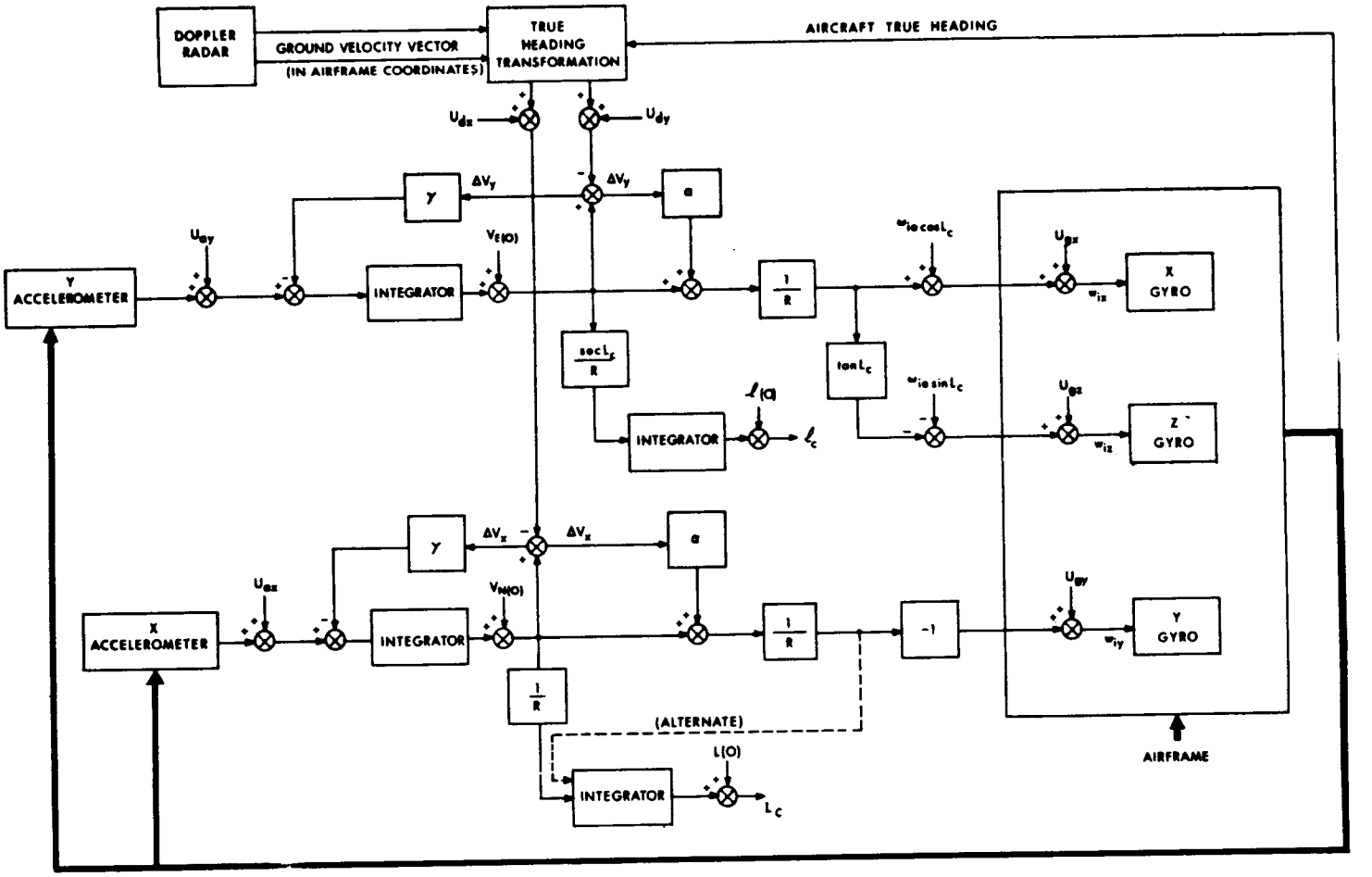


Fig. 5 Mechanization of Inertial-Doppler Navigator, Showing Entry of Instrumentation Uncertainties

(f) Dynamics of the space integrator are neglected.

Define three coordinate frames as follows:

Inertial (i) frame - origin at the aircraft, nonrotating with respect to inertial space.

Navigational (n) frame - origin at the aircraft, axes in directions of true north (N), east (E), and the geographic vertical.

Computational (c) frame - origin at the aircraft, axes (x, y, z) defined by the input axes of platform's gyros. It is assumed that the gyro input axes are mutually orthogonal, and that the accelerometer sensitive axes coincide with the x and y gyro input axes.

The inertial navigator is of the semi-geometric configuration, so that following initial alignment the navigational and computational frames are nearly coincident. Define the correction angles $C_x$, $C_y$, $C_z$ as the angles of rotation about the x, y, and z axes required to bring the computational frame into coincidence with the navigational frame. Pictorial representation of $C_x$, $C_y$, and $C_z$ is shown in reference (9). These correction angles will be time varying. Adopting the notation convention $\vec{r}^{\,c} = C_n^c \vec{r}^{\,n}$, the transformation matrix $C_n^c$ assuming the correction angles to be small becomes

$$C_n^c = \begin{pmatrix} 1 & -C_z & C_y \\ C_z & 1 & -C_x \\ -C_y & C_x & 1 \end{pmatrix}$$

The specific force sensed by the accelerometers is $\vec{f}^{\,c} = C_i^c \ddot{\vec{r}}^{\,i} - \vec{G}^c$.

Coriolis and centripetal acceleration terms are assumed to be perfectly cancelled by computed acceleration compensation terms, so that

$$\vec{f}^{\,c} = C_n^c \left[ \ddot{\vec{r}}^{\,n} - \vec{g}^{\,n} \right] = \begin{pmatrix} 1 & -C_z & C_y \\ C_z & 1 & -C_x \\ -C_y & C_x & 1 \end{pmatrix} \left[ \begin{pmatrix} \ddot{r}_N \\ \ddot{r}_E \\ \ddot{r}_V \end{pmatrix} - \begin{pmatrix} o \\ o \\ g \end{pmatrix} \right].$$

If the aircraft is maintaining constant altitude, groundspeed, and track angle, then

$\ddot{\vec{r}}^{c} = 0$ by the assumption of perfect application of coriolis compensation and

$$\vec{f}^{c} = \begin{pmatrix} -gC_y \\ gC_x \\ -g \end{pmatrix}.$$

The gyro input axes will have an angular velocity with respect to inertial space of $\vec{\omega}^{c}_{ic}$, where

$$\vec{\omega}^{c}_{ic} = \vec{\omega}^{c}_{ie} + \vec{\omega}^{c}_{en} + \vec{\omega}^{c}_{nc} = C^{c}_{n}\vec{\omega}^{n}_{ie} + C^{c}_{n}\vec{\omega}^{n}_{en} + \vec{\omega}^{c}_{nc}$$

$$= \begin{pmatrix} 1 & -C_z & C_y \\ C_z & 1 & -C_x \\ -C_y & C_x & 1 \end{pmatrix} \begin{pmatrix} \omega_{ie}\cos L \\ 0 \\ -\omega_{ie}\sin L \end{pmatrix} + \begin{pmatrix} 1 & -C_z & C_y \\ C_z & 1 & -C_x \\ -C_y & C_x & 1 \end{pmatrix} \begin{pmatrix} \frac{V_E}{R} \\ \frac{-V_N}{R} \\ \frac{V_E}{R}\tan L \end{pmatrix} - \begin{pmatrix} \dot{C}_x \\ \dot{C}_y \\ \dot{C}_z \end{pmatrix}$$

$$= \begin{pmatrix} \omega_{ie}\cos L - C_y\omega_{ie}\sin L + \frac{V_E}{R} + C_z\frac{V_N}{R} - C_y\frac{V_E}{R}\tan L - \dot{C}_x \\ C_z\omega_{ie}\cos L + C_x\omega_{ie}\sin L + C_z\frac{V_E}{R} - \frac{V_N}{R} + C_x\frac{V_E}{R}\tan L - \dot{C}_y \\ -C_y\omega_{ie}\cos L - \omega_{ie}\sin L - C_y\frac{V_E}{R} - C_x\frac{V_N}{R} - \frac{V_E}{R}\tan L - \dot{C}_z \end{pmatrix}$$

Taking the Laplace transform,

$$\overline{\vec{\omega}^{c}_{ic}} \equiv \mathcal{L}\left\{\vec{\omega}^{c}_{ic}\right\} = \begin{pmatrix} \frac{\omega_{ie}\cos L}{p} - \bar{C}_y\omega_{ie}\sin L + \frac{V_E}{pR} + \bar{C}_z\frac{V_N}{R} - \bar{C}_y\frac{V_E}{R}\tan L - p\bar{C}_x + C_x(0) \\ \bar{C}_z\omega_{ie}\cos L + \bar{C}_x\omega_{ie}\sin L + \bar{C}_z\frac{V_E}{R} - \frac{V_N}{pR} + \bar{C}_x\frac{V_E}{R}\tan L - p\bar{C}_y + C_y(0) \\ -\bar{C}_y\omega_{ie}\cos L - \frac{\omega_{ie}\sin L}{p} - \bar{C}_y\frac{V_E}{R} - \bar{C}_x\frac{V_N}{R} - \frac{V_E}{pR}\tan L - p\bar{C}_z + C_z(0) \end{pmatrix} \quad (1)$$

After resolution about the inertial system's true heading angle, the doppler-derived ground velocity components in the computational frame are

$$C_n^c \begin{pmatrix} V_N \\ V_E \\ 0 \end{pmatrix} + \begin{pmatrix} U_{dx} \\ U_{dy} \\ 0 \end{pmatrix} = \begin{pmatrix} V_N - C_z V_E + U_{dx} \\ V_E + C_z V_N + U_{dy} \\ 0 \end{pmatrix}$$

where $U_{dx}$ and $U_{dy}$ are the uncertainites in the radar's velocity determination. These uncertainties may be partially dependent on the dynamics of the doppler frequency tracker, wind, aircraft maneuvers, speed, and the nature of the surface overflown, and will be determined by the specific design of the radar.

The total angular velocity with respect to inertial space that is commanded to the gyro floats (including gyro uncertainties $U_{gx}$, $U_{gy}$, and $U_{gz}$), is

$$\vec{W}_{ic}^{c} = \left(W_{ix}, W_{iy}, W_{iz}\right).$$

Space integrator dynamics are neglected i.e., the actual angular velocity of the controlled member with respect to inertial space is at all times equal to that commanded of the gyro floats: $\vec{\omega}_{ic} = \vec{W}_{ic}$.

The correction to computed latitude $C_L$ is defined as

$$C_L \triangleq L - L_c .$$

The signal flow diagram of the x-axis computational channel is shown in Figure 6. From this diagram, the Laplace transform of computed latitude is derived using Mason's generalized gain formula (reference (10)) as

$$\overline{L}_c = \frac{1}{Rp\left(1+\frac{\gamma}{p}\right)}\left(\frac{-g\overline{C}_x}{p} + \frac{\overline{U}_{ax}}{p} + \frac{\gamma}{p}\left(\frac{V_N}{p} - V_E\overline{C}_z + \overline{U}_{dx}\right) + \frac{V_N(0)}{p}\right) + \frac{L(0)}{p}$$

The Laplace transform of actual latitude is

$$\overline{L} = \frac{L(0)}{p} + \frac{V_N}{p^2 R} \quad \text{where}$$

initial latitude L(0) is assumed to be known precisely. Recognizing that $V_N \equiv V_N(0)$ since $V_N(t)$ = constant, an expression for the Laplace transform of the correction to computed latitude is obtained:

$$\overline{C}_L = \frac{1}{p(p+\gamma)R}\left(g\overline{C}_y + \gamma V_E\overline{C}_z - \overline{U}_{ax} - \gamma\overline{U}_{dx}\right) \qquad (2)$$

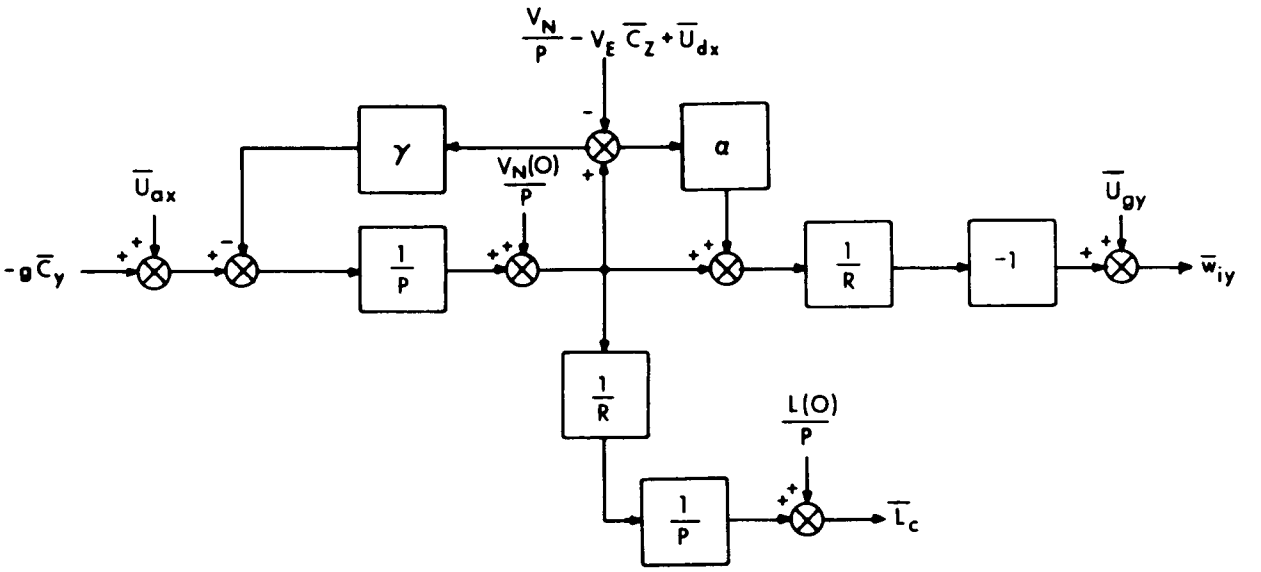


Fig. 6 Signal Flow Diagram Showing Computation of Latitude and Y-Axis Component of $\vec{W}_{ic}^{c}$

Assuming $C_L$ to always be a small angle, the following trigonometric relationships are valid:

$$\sin L_c \cong \sin L - C_L \cos L \tag{3}$$

$$\cos L_c \cong \cos L + C_L \sin L \tag{4}$$

$$\tan L_c \cong \tan L - C_L \sec^2 L \tag{5}$$

$$\sec L_c \cong \sec L - C_L \sec L \tan L \tag{6}$$

From Figure 6, the total command to the space integrator for the component of angular velocity with respect to inertial space about the y-axis is

$$\bar{W}_{iy} = \frac{-1}{R(1+\frac{\gamma}{p})}\left[-\left(\frac{1+\alpha}{p}\right) g\bar{C}y + \left(\frac{1+\alpha}{p}\right)\bar{U}_{ax} + \left(\frac{\gamma}{p} - \alpha\right)\left(\frac{V_N}{p} - V_E\bar{C}_z + \bar{U}_{dx}\right) + \right.$$

$$\left. + (1+\alpha)\frac{V_{N(o)}}{p}\right] + \bar{U}_{gy}$$

Defining

$$\omega_s{}^2 \triangleq \frac{g}{R}$$

and

$$K \triangleq 1+\alpha$$

then,

$$\bar{W}_{iy} = \frac{-V_N}{pR} + \frac{K\omega_s{}^2}{p+\gamma}\bar{C}_y + \frac{V_E}{R}\bar{C}_z - \frac{pKV_E}{(p+\gamma)R}\bar{C}_z + \bar{U}_{gy} - \frac{K}{(p+\gamma)R}\bar{U}_{ax} -$$

$$\frac{1}{R}\bar{U}_{dx} + \frac{pK}{(p+\gamma)R}\bar{U}_{dx} \tag{7a}$$

Similarly, from Figure 7, equations (3), (4), and (5), and neglecting terms having products of small quantities (corrections and uncertainties),

$$\bar{W}_{ix} = \frac{\omega_{ie}\cos L}{p} + \frac{V_E}{pR} + \frac{K\omega_s{}^2}{p+\gamma}\bar{C}_x + \frac{\omega_s{}^2\,\omega_{ie}\sin L}{p(p+\gamma)}\bar{C}_y + \frac{\gamma\omega_{ie}V_E\sin L}{p(p+\gamma)R}\bar{C}_z +$$

$$+ \frac{V_N}{R}\bar{C}_z - \frac{pKV_N}{(p+\gamma)R}\bar{C}_z + \bar{U}_{gx} - \frac{\omega_{ie}\sin L}{p(p+\gamma)R}\bar{U}_{ax} +$$

$$+ \frac{K}{(p+\gamma)R}\bar{U}_{ay} - \frac{\gamma\omega_{ie}\sin L}{p(p+\gamma)R}\bar{U}_{dx} + \frac{1}{R}\bar{U}_{dy}\frac{-pK}{(p+\gamma)R}\bar{U}_{dy} \tag{7b}$$

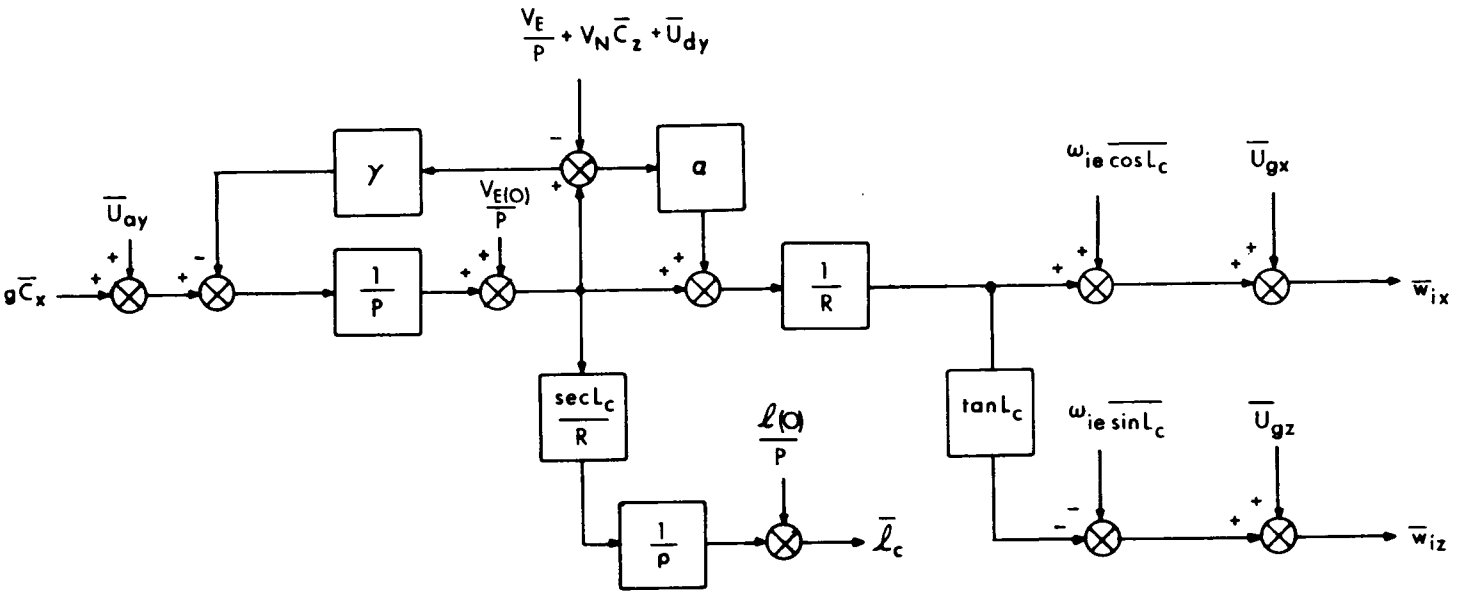


Fig. 7 Signal Flow Diagram Showing Computation of Longitude and X-Axis and Z-Axis Components of $\vec{W}_{ic}^{c}$

$$\overline{W}_{iz} = \frac{-\omega_{ie} \sin L}{p} - \frac{V_E \tan L}{pR} - \frac{K\omega_s^2 \tan L}{p+\gamma} \overline{C}_x + \frac{\omega_s^2 \omega_{ie} \cos L}{p(p+\gamma)} \overline{C}_y$$

$$+ \frac{\omega_s^2 V_E \sec^2 L}{p(p+\gamma)R} \overline{C}_y + \frac{\gamma\omega_{ie} V_E \cos L}{p(p+\gamma)R} \overline{C}_z -$$

$$- \frac{V_N}{R} \tan L \, \overline{C}_z + \frac{pKV_N \tan L}{(p+\gamma)R} \overline{C}_z + \frac{\gamma V_E^2 \sec^2 L}{p(p+\gamma)R^2} \overline{C}_z +$$

$$+ \overline{U}_{gz} - \frac{\omega_{ie} \cos L}{p(p+\gamma)R} \overline{U}_{ax} - \frac{V_E \sec^2 L}{p(p+\gamma)R^2} \overline{U}_{ax} - \frac{K \tan L}{(p+\gamma)R} \overline{U}_{ay} -$$

$$- \frac{\gamma\omega_{ie} \cos L}{p(p+\gamma)R} \overline{U}_{dx} - \frac{\gamma V_E \sec^2 L}{p(p+\gamma)R^2} \overline{U}_{dx} - \frac{\tan L}{R} \overline{U}_{dy} +$$

$$+ \frac{pK \tan L}{(p+\gamma)R} \overline{U}_{dy} \qquad (7c)$$

Equating ( 1) and (7), the performance equation set for the space integrator is obtained. Simplifying algebraically and putting in matrix form, equation (8) results. This is of the form

$$\left[A\right] \left[C_v\right] = \left[F_1\right] \left[U\right] \qquad (8')$$

where $\left[C_v\right]$ is the matrix of space integrator controlled member correction angles, and $\left[U\right]$ the sensor uncertainties.

$$
\begin{bmatrix}
p^2\left(p^2+\gamma p+K\omega_s^2\right) & \left(\omega_{ie}\sin L+\frac{V_E}{R}\tan L\right)p^3 & \frac{-KV_N}{R}p^3+\gamma\omega_{ie}\frac{V_E}{R}\sin L\,p \\
& +\gamma\left(\omega_{ie}\sin L+\frac{V_E}{R}\tan L\right)p^2 & \\
& +\omega_s^2\,\omega_{ie}\sin L\,p & \\
-\left(\omega_{ie}\sin L+\frac{V_E}{R}\tan L\right)p^3 & p^2\left(p^2+\gamma p+K\omega_s^2\right) & -\left(\omega_{ie}\cos L+\frac{KV_E}{R}\right)p^3 \\
-\gamma\left(\omega_{ie}\sin L+\frac{V_E}{R}\tan L\right)p^2 & & -\gamma\omega_{ie}\cos L\,p^2 \\
\frac{V_N}{R}p^3+\left(\gamma\frac{V_N}{R}-K\omega_s^2\tan L\right)p & \left(\omega_{ie}\cos L+\frac{V_E}{R}\right)p^3 & p^4+\left(\gamma+\frac{(K-1)V_N}{R}\tan L\right)p^3 \\
& +\gamma\left(\omega_{ie}\cos L+\frac{V_E}{R}\right)p^2 & -\gamma\frac{V_N}{R}\tan L\,p^2 \\
& +\omega_s^2\left(\omega_{ie}\cos L+\frac{V_E}{R}\sec^2 L\right)p & +\gamma\frac{V_E}{R}\left(\omega_{ie}\cos L+\frac{V_E}{R}\sec^2 L\right)p
\end{bmatrix}
\begin{bmatrix}\overline{C}_x\\ \overline{C}_y\\ \overline{C}_z\end{bmatrix}
=
$$

$$
\begin{bmatrix}
p^3+\gamma p^2 & 0 & 0 & -p^3-\gamma p^2 & 0 & 0 & \frac{\omega_{ie}\sin L}{R}p & \frac{-K}{R}p^2 & \frac{\gamma\omega_{ie}\sin L}{R}p & \frac{(K-1)}{R}p^3-\frac{\gamma}{R}p^2 \\
0 & p^3+\gamma p^2 & 0 & 0 & -p^3-\gamma p^2 & 0 & \frac{K}{R}p^2 & 0 & \frac{-(K-1)}{R}p^3+\frac{\gamma}{R}p^2 & 0 \\
0 & 0 & p^3-\gamma p^2 & 0 & 0 & -p^3-\gamma p^2 & \left(\frac{\omega_{ie}\cos L+\frac{V_E}{R}\sec^2 L}{R}\right)p & \frac{K\tan L}{R}p^2 & \gamma\left(\frac{\omega_{ie}\cos L+\frac{V_E}{R}\sec^2 L}{R}\right)p & \frac{-(K-1)\tan L}{R}p^3+\frac{\gamma}{R}\tan L\,p^2
\end{bmatrix}
\begin{bmatrix}
C_x(0)\\ C_y(0)\\ C_z(0)\\ \overline{U}_g\\ \overline{U}_{gy}\\ \overline{U}_{gz}\\ \overline{U}_{ax}\\ \overline{U}_{ay}\\ \overline{U}_{dx}\\ \overline{U}_{dy}
\end{bmatrix}
\qquad (8)
$$

1. Stationary System

In the case of a system stationary on the earth, $V_N = V_E = 0$. The characteristic equation of the system is then

$$\Delta = \det[A] = 0$$

or

$$p^5(p+\gamma)\left(p^2+\gamma p+K\omega_s^2\right)\left(p^4+\gamma p^3+\left(K\omega_s^2+\omega_{ie}^2\right)p^2+\gamma\omega_{ie}^2 p+\omega_s^2\omega_{ie}^2\right)=0$$

Since $\gamma > 0$ and $K > 1$, Routh's criterion (reference (11)) shows the roots of the quartic factor to all have negative real parts. Thus both the Schuler mode and the earth rate mode are damped; effectiveness of this damping is not given by Routh's criterion. The natural frequency of one Schuler mode has been increased from $\omega_s$ to $\sqrt{K}\,\omega_s$, so that the Schuler oscillations are not only damped (the damping ratio of the quadratic term is $\frac{\gamma}{2\sqrt{K}\,\omega_s}$), but the period has been decreased to $\sqrt{K}$ 84 minutes.

A stable system is also possible if $\gamma > 0$ but $K = 1$ ( the gain $\alpha$ is zero). Then the characteristic equation becomes

$$\Delta = p^5(p+\gamma)\left(p^2+\gamma p+\omega_s^2\right)^2\left(p^2+\omega_{ie}^2\right)=0.$$

Both Schuler modes are damped as before, but not changed in period. The earth rate mode oscillates undamped.

A third possibility lies in choosing a different signal representation of northerly velocity to drive the computed latitude integrator. If computed latitude is derived from the computed y-gyro command angular velocity, shown by the alternate connection in Figure 5, the derivation of the space integrator performance equation set is similar to that given above. The result is that the characteristic equation (again assuming a stationary system) is then

$$\Delta = p^5(p+\gamma)\left(p^2+\gamma p+K\omega_s^2\right)^2\left(p^2+\omega_{ie}^2\right).$$

Both Schuler modes are equally speeded up and damped, and the earth rate mode oscillates undamped.

Returning to the basic system of Figure 5, the effect of inaccuracies in initial geometric alignment of the space integrator controlled member (failure to match the computational frame to the navigational frame prior to system operation) and uncertainties in gyros and in doppler radar operation are obtained as solutions of equation set (8). The Laplace transforms of controlled member correction angles as functions of gyro and doppler uncertainty for the stationary system are the following:

$$\bar{C}_x = \frac{\begin{aligned}&(p+\gamma)\left[p^2\left(p^2+\gamma p+K\omega_s^2\right)+\omega_{ie}^2\cos^2 L\left(p^2+\gamma p+\omega_s^2\right)\right]\left[C_x(0)-\bar{U}_{gx}\right]+\\&-\left[\omega_{ie}\sin L\, p\,(p+\gamma)\left(p^2+\gamma p+\omega_s^2\right)\right]\left[C_y(0)-\bar{U}_{gy}\right]+\\&-\left[\omega_{ie}^2\sin L\cos L\,(p+\gamma)\left(p^2+\gamma p+\omega_s^2\right)\right]\left[C_z(0)-\bar{U}_{gz}\right]+\\&+\left\{\omega_{ie}\sin L\,(K-1)\,p\left[p^2+\gamma p+(\gamma+1)\,\omega_s^2\right]\right\}\frac{\bar{U}_{dx}}{R}+\\&+\left\{p^2\left(p^2+\gamma p+K\omega_s^2\right)+\omega_{ie}^2\left(p^2+\gamma p+\omega_s^2\right)\left[(K-1)\,p-\gamma\right]\right\}\frac{\bar{U}_{dy}}{R}\end{aligned}}{\left(p^2+\gamma p+K\omega_s^2\right)\left(p^4+\gamma p^3+\left(K\omega_s^2+\omega_{ie}^2\right)p^2+\gamma\omega_{ie}^2\,p+\omega_s^2\,\omega_{ie}^2\right)}$$

$$\bar{C}_y = \frac{\begin{aligned}&\left[\omega_{ie}\sin L\,p\,(p+\gamma)\right]\left[C_x(0)-\bar{U}_{gx}\right]+\left[p^2\,(p+\gamma)\right]\left[C_y(0)-\bar{U}_{gy}\right]+\\&+\left[\omega_{ie}\cos L\,p\,(p+\gamma)\right]\left[C_z(0)-\bar{U}_{gz}\right]\\&+\left[(1-K)\,p^3+\gamma p^2+\gamma\omega_{ie}^2\right]\frac{\bar{U}_{dx}}{R}\end{aligned}}{p^4+\gamma p^3+\left(K\omega_s^2+\omega_{ie}^2\right)p^2+\gamma\omega_{ie}^2\,p+\omega_s^2\,\omega_{ie}^2}$$

$$\bar{C}_z = \frac{\begin{aligned}&(p+\gamma)\left[K\omega_s^2\tan L\,p\left(p^2+\gamma p+K\omega_s^2\right)-\omega_{ie}^2\sin L\cos L\,(p+\gamma)\left(p^2+\gamma p+\omega_s^2\right)\right]\left[C_x(0)-\bar{U}_{gx}\right]+\\&-(p+\gamma)\left[\omega_{ie}\left(p^2+\gamma p+\omega_s^2\right)\left(\left(p^2+\gamma p+K\omega_s^2\right)\cos L+K\omega_s^2\sin L\tan L\right)\right]\left[C_y(0)-\bar{U}_{gy}\right]+\\&+(p+\gamma)\left[p\left(p^2+\gamma p+K\omega_s^2\right)^2+\omega_{ie}^2\sin^2 L\,(p+\gamma)\left(p^2+\gamma p+\omega_s^2\right)\right]\left[C_z(0)-\bar{U}_{gz}\right]+\\&+\left\{\gamma K\omega_s^2\,\omega_{ie}\sin L\tan L\left(p^2+\gamma p+K\omega_s^2\right)+\right.\\&\omega_{ie}\left(p^2+\gamma p+\omega_s^2\right)\left[\left(p^2+\gamma p+K\omega_s^2\right)\cos L+K\omega_s^2\sin L\tan L\right]\left[(K-1)p-\gamma\right]+\\&\left.+\gamma\omega_{ie}\cos L\left(p^2+\gamma p+K\omega_s^2\right)^2\right\}\frac{\bar{U}_{dx}}{R}+\\&+\left\{\left[-\omega_{ie}^2(p+\gamma)\left(p^2+\gamma p+\omega_s^2\right)-p^2(p+\gamma)\left(p^2+\gamma p+K\omega_s^2\right)\right]\left[(K-1)\,p-\gamma\right]\tan L\right\}\frac{\bar{U}_{dy}}{R}\end{aligned}}{(p+\gamma)\left(p^2+\gamma p+K\omega_s^2\right)\left(p^4+\gamma p^3+(K\omega_s^2+\omega_{ie}^2)\,p^2+\gamma\omega_{ie}^2\,p+\omega_s^2\,\omega_{ie}^2\right)}$$

2. Nonstationary System

Both the characteristic matrix A and the forcing function matrix $F_1$ are functions of aircraft velocity. An initial analysis could proceed on the basis of a stationary system, as above. However a more realistic result follows if effects of aircraft velocity are included. This is particularly true in an application such as the SST, where the angular velocity of the aircraft relative to the earth will exceed that of the earth relative to inertial space. In this situation an explicit general solution for the components of the platform correction angle matrix is not practical since the characteristic equation $\Delta = \det A = 0$ is not easily factorable. A numerical solution relative to any particular situation could be calculated, preferably by digital computer.

## 3. Navigational Errors

The primary navigational data from the system is aircraft true heading and present position, expressed as geographic latitude and longitude. True heading is measurable directly using the z-axis of the space integrator as a reference. Computed latitude and longitude are obtained as shown in figure 5. As before, $C_Z$ is the correction to space integrator true heading angle, and $C_L$ the correction to computed latitude

$$C_L \triangleq L - L_c$$

Similarly, $C_\ell$ is defined as the correction to computed longitude

$$C_\ell \triangleq \ell - \ell_c$$

Repeating equation (2), the Laplace transform of $C_L$ is

$$C_L = \frac{1}{p(p+\gamma)R}\left(g\bar{C}y + \gamma V_E \bar{C}_Z - \bar{U}_{ax} - \gamma \bar{U}_{dx}\right) \tag{2}$$

From figure 7 and equation (6), neglecting products of $C_L$ with other small quantities,

$$\bar{C}_\ell = \frac{\sec L}{p(p+\gamma)R}\left(-g\bar{C}x - \gamma V_N \bar{C}_Z - \bar{U}_{ay} - \gamma \bar{U}_{dy}\right) \tag{11}$$

$\bar{C}_L$, $\bar{C}_\ell$, and $\bar{C}_Z$ are the elements of the navigational correction matrix $[C_N]$ which by (2), (11), and the appropiate elements of (8) is related to the space integrator correction matrix $[C_v]$ and sensor uncertainty matrix $[U]$ by the following:

$$\begin{bmatrix} \bar{C}_L \\ C_\ell \\ C_z \end{bmatrix} = \begin{bmatrix} 0 & \frac{\omega_s^2}{p(p+\gamma)} & \frac{\gamma V_E}{p(p+\gamma)R} \\ \frac{-\omega_s^2 \sec L}{p(p+\gamma)} & 0 & \frac{-\gamma V_N \sec L}{p(p+\gamma)} \\ 0 & 0 & 1 \end{bmatrix} \begin{bmatrix} \bar{C}_x \\ \bar{C}_y \\ \bar{C}_z \end{bmatrix} + \begin{bmatrix} 0 & 0 & 0 & \frac{-1}{p(p+\gamma)R} & 0 & \frac{-\gamma}{p(p+\gamma)R} & 0 \\ 0 & 0 & 0 & 0 & \frac{-\sec L}{p(p+\gamma)R} & 0 & \frac{-\gamma \sec L}{p(p+\gamma)R} \\ 0 & 0 & 0 & 0 & 0 & 0 & 0 \end{bmatrix} \begin{bmatrix} \bar{U}_{gx} \\ \bar{U}_{gy} \\ \bar{U}_{gz} \\ \bar{U}_{ax} \\ \bar{U}_{ay} \\ \bar{U}_{dx} \\ \bar{U}_{dy} \end{bmatrix} \tag{12}$$

This is of the form

$$[C_N] = [B][C_v] + [F_2][U].$$

The determinant of $[B]$ is $\frac{\omega_s^4 \sec L}{p^2(p+\gamma)^2} \neq 0$. Thus $[B]$ is nonsingular and possesses a unique inverse. Manipulating matrix equations (8) and (12) yields equation (13) which relates sensor uncertainties to error in the navigational outputs of the system.

$$[A][B]^{-1}[C_N] = \left[[F_1] + [A][B]^{-1}[F_2]\right][U]. \tag{13'}$$

$$
\begin{bmatrix}
\left[\begin{matrix}\left(\omega_{ie}\sin L + \frac{V_E}{R}\tan L\right)p^2 \\ +\gamma\left(\omega_{ie}\sin L + \frac{V_E}{R}\tan L\right)p \\ +\omega_s^2\ \omega_{ie}\sin L\end{matrix}\right] \times \frac{p^2(p+\gamma)}{\omega_s^2} & -\left[p^2+\gamma p+K\omega_s^2\right] \times \frac{p^3(p+\gamma)}{\omega_s^2}\cos L & \begin{matrix}\frac{-\gamma V_N}{\omega_s^2 R}\,p^4 \\ -\left\{\frac{\gamma}{\omega_s^2}\left[\frac{\gamma V_N}{R}+\frac{V_E}{R}\left(\omega_{ie}\sin L+\frac{V_E}{R}\tan L\right)\right]+K\frac{V_N}{R}\right\}p^3 \\ -\gamma\left[\frac{KV_N}{R}+\frac{\gamma V_E}{\omega_s^2 R}\left(\omega_{ie}\sin L+\frac{V_E}{R}\tan L\right)\right]p^2\end{matrix} \\
\left[p\left(p^2+\gamma p+K\omega_s^2\right)\right] \times \frac{p^2(p+\gamma)}{\omega_s^2} & \left[\begin{matrix}\left(\omega_{ie}\sin L+\frac{V_E}{R}\tan L\right)p \\ +\gamma\left(\omega_{ie}\sin L+\frac{V_E}{R}\tan L\right)\end{matrix}\right] \times \frac{p^3(p+\gamma)}{\omega_s^2}\cos L & \begin{matrix}\frac{-\gamma V_E}{\omega_s^2 R}\,p^4 \\ +\left[\frac{\gamma V_N}{\omega_s^2 R}\left(\omega_{ie}\sin L+\frac{V_E}{R}\tan L\right)-\frac{\gamma^2 V_E}{\omega_s^2 R}-\omega_{ie}\cos L-K\frac{V_E}{R}\right]p^3 \\ +\left[\frac{\gamma^2 V_N}{\omega_s^2 R}\left(\omega_{ie}\sin L+\frac{V_E}{R}\tan L\right)-\frac{\gamma K V_E}{R}-\gamma\omega_{ie}\cos L\right]p^2\end{matrix} \\
\left[\begin{matrix}\left(\omega_{ie}\cos L+\frac{V_E}{R}\right)p^2 \\ +\gamma\left(\omega_{ie}\cos L+\frac{V_E}{R}\right)p \\ +\omega_s^2\left(\omega_{ie}\cos L+\frac{V_E}{R}\sec^2 L\right)\end{matrix}\right] \times \frac{p^2(p+\gamma)}{\omega_s^2} & -\left[\frac{V_N}{R}p+\left(\gamma\frac{V_N}{R}-K\omega_s^2\tan L\right)\right] \times \frac{p^3(p+\gamma)}{\omega_s^2}\cos L & \begin{matrix}p^4+\left[\frac{-\gamma V_N^2}{\omega_s^2 R^2}-\frac{\gamma V_E}{\omega_s^2 R}\left(\omega_{ie}\cos L+\frac{V_E}{R}\right)+\gamma+\frac{(K-1)V_N}{R}\tan L\right]p^3 \\ +\left[\frac{-\gamma^2 V_N^2}{\omega_s^2 R^2}+\frac{\gamma(K-1)V_N\tan L}{R}-\frac{\gamma^2 V_E}{\omega_s^2 R}\left(\omega_{ie}\cos L+\frac{V_E}{R}\right)\right]p^2\end{matrix}
\end{bmatrix}
\begin{bmatrix}\overline{C}_L \\ \overline{C}_\ell \\ \overline{C}_z\end{bmatrix} =
$$

$$
\begin{bmatrix}
p^2(p+\gamma) & 0 & 0 & -p^2(p+\gamma) & 0 & 0 & \frac{-1}{\omega_s^2 R}\left(\omega_{ie}\sin L + \frac{V_E}{R}\tan L\right)p^3 & \frac{1}{\omega_s^2 R}p^4 + \frac{\gamma}{\omega_s^2 R}p^3 & \frac{-\gamma}{\omega_s^2 R}\left(\omega_{ie}\sin L + \frac{V_E}{R}\tan L\right)p^3 & \frac{\gamma}{\omega_s^2 R}p^4 + \frac{1}{R}\left(\frac{\gamma^2}{\omega_s^2} + K - 1\right)p^3 \\
 & & & & & & -\frac{\gamma}{\omega_s^2 R}\left(\omega_{ie}\sin L + \frac{V_E}{R}\tan L\right)p^2 & & \frac{\gamma^2}{\omega_s^2 R}\left(\omega_{ie}\sin L + \frac{V_E}{R}\tan L\right)p^2 & + \frac{\gamma}{R}(K-1)p^2 \\
0 & p^2(p+\gamma) & 0 & 0 & -p^2(p+\gamma) & 0 & \frac{-1}{\omega_s^2 R}\left(\omega_{ie}\sin L + \frac{V_E}{R}\tan L\right)p^3 & \frac{-\gamma}{\omega_s^2 R}p^4 - \frac{1}{R}\left(\frac{\gamma^2}{\omega_s^2} + K - 1\right)p^3 & \frac{-\gamma}{\omega_s^2 R}\left(\omega_{ie}\sin L + \frac{V_E}{R}\tan L\right)p^3 & \\
 & & & & & & -\frac{\gamma}{\omega_s^2 R}\left(\omega_{ie}\sin L + \frac{V_E}{R}\tan L\right)p^2 & -\frac{\gamma}{R}(K-1)p^2 & -\frac{\gamma^2}{\omega_s^2 R}\left(\omega_{ie}\sin L + \frac{V_E}{R}\tan L\right)p^2 & \\
0 & 0 & p^2(p+\gamma) & 0 & 0 & -p^2(p+\gamma) & \frac{-1}{\omega_s^2 R}\left(\omega_{ie}\cos L + \frac{V_E}{R}\right)p^3 & \frac{V_N}{\omega_s^2 R^2}p^3 + \frac{\gamma V_N}{\omega_s^2 R^2}p^2 & \frac{-\gamma}{\omega_s^2 R}\left(\omega_{ie}\cos L + \frac{V_E}{R}\right)p^3 & \frac{1}{R}\left[\frac{\gamma V_N}{\omega_s^2 R} - (K-1)\tan L\right]p^3 \\
 & & & & & & -\frac{\gamma}{\omega_s^2 R}\left(\omega_{ie}\cos L + \frac{V_E}{R}\right)p^2 & & -\frac{\gamma^2}{\omega_s^2 R}\left(\omega_{ie}\cos L + \frac{V_E}{R}\right)p^2 & + \frac{\gamma}{R}\left[\frac{\gamma V_N}{\omega_s^2 R} - (K-1)\tan L\right]p^2
\end{bmatrix}
\begin{bmatrix}
C_x(0) \\ C_y(0) \\ C_z(0) \\ \bar{U}_{gx} \\ \bar{U}_{gy} \\ \bar{U}_{gz} \\ \bar{U}_{ax} \\ \bar{U}_{ay} \\ \bar{U}_{dx} \\ \bar{U}_{dy}
\end{bmatrix}
\tag{13}
$$

Gyrocompassing Mechanization

An extension of the doppler damped inertial navigator discussed so far would be a form of moving base gyrocompassing system. A possible configuration, suggested in references (2) and (3), is identical to that shown in Figure 5 but with the addition of an angular velocity command to the z-axis of the space integrator derived from the x-axis linear velocity error signal $\Delta V_x$. The added $W_{iz}$ term is

$$\frac{G\,\Delta V_x}{R}\,\mathrm{secL_c}$$

where G is a constant gain, R converts linear to angular velocity about the earth, and the $\mathrm{secL_c}$ factor is intended to reduce the dependence of system dynamics on latitude. For the case of operation stationary on the earth with no doppler input, the system reduces to a velocity coupled gyrocompass, a connection frequently used to effect initial alignment of the space integrator axes prior to flight. If the gyrocompassing connection is retained during flight the x-axis component of doppler-sensed velocity (of the aircraft relative to the earth) should exactly cancel the inertially sensed x-axis component of velocity. Any residual $\Delta V_x$ signal is attributed to earth rate felt about the y-axis because of a non-zero $C_z$ angle. Thus it is argued that the added $W_{iz}$ term will quickly limit $C_z$ by continuous gyrocompassing action.

The previous three-axis matrix equation set developed for the system of Figure 5 may be easily modified to include the added gyrocompassing term. From Figure 7 the Laplace transform of the north velocity error signal $\Delta V_x$ is

$$\Delta\overline{V}_x = \frac{1}{\left(1+\frac{\gamma}{p}\right)}\left[\frac{V_{N(o)}}{p} - \left(\frac{V_N}{p} - V_E\overline{C}_z + \overline{U}_{dx}\right) + \frac{1}{p}\,\overline{U}_{ax} - \frac{1}{p}\,g\overline{C}_y\right]$$

$$= \frac{1}{\gamma+p}\left[-g\overline{C}_y + pV_E\overline{C}_z\right] + \frac{1}{\gamma+p}\left[\overline{U}_{ax} - p\overline{U}_{dx}\right]$$

Using equation (6), the previous expression for $W_{iz}$ (7c) is augmented by the additional terms

$$\frac{G\,\mathrm{secL}}{R(p+\gamma)}\left[-g\overline{C}y + pV_E\overline{C}_z\right] + \frac{G\,\mathrm{secL}}{R(p+\gamma)}\left[\overline{U}_{ax} - p\overline{U}_{dx}\right]$$

By equating $\vec{\omega}^{c}_{ic} = \vec{W}^{c}_{ic}$ as before, a matrix equation analogous to (8) may be obtained. The characteristic matrix of the system is given in Figure 8 for reference.

For the algebraically simple case of pure easterly velocity at the equator, rotation about the space integrator's x axis is decoupled from the y and z axes. The characteristic equation of the gyrocompass then becomes

$$
\begin{bmatrix}
p^2\left(p^2+\gamma p+K\omega_s^2\right) & \left(\omega_{ie}\sin L+\frac{V_E}{R}\tan L\right)p^3 & -K\frac{V_N}{R}p^3 \\
 & +\gamma\left(\omega_{ie}\sin L+\frac{V_E}{R}\tan L\right)p^2 & +\gamma\omega_{ie}\frac{V_E}{R}\sin Lp \\
 & +\omega_s^2\,\omega_{ie}\sin L\,p & \\
 & & \\
-\left(\omega_{ie}\sin L+\frac{V_E}{R}\tan L\right)p^3 & p^2\left(p^2+\gamma p+K\omega_s^2\right) & -\left(\omega_{ie}\cos L+K\frac{V_E}{R}\right)p^3 \\
-\gamma\left(\omega_{ie}\sin L+\frac{V_E}{R}\tan L\right)p^2 & & -\gamma\omega_{ie}\cos L\,p^2 \\
 & & \\
\frac{V_N}{R}p^3+\left(\gamma\frac{V_N}{R}-K\omega_s^2\tan L\right)p^2 & \left(\omega_{ie}\cos L+\frac{V_E}{R}\right)p^3 & p^4+\left(\gamma+\frac{(K-1)\,V_N\tan L}{R}+\omega_s^2\,\frac{GV_E\sec L}{R}\right)p^3 \\
 & +\left[\gamma\left(\omega_{ie}\cos L+\frac{V_E}{R}\right)-\omega_s^2\,G\sec L\right]p^2 & -\gamma\frac{V_N}{R}\tan L\,p^2 \\
 & +\omega_s^2\left(\omega_{ie}\cos L+\frac{V_E}{R}\sec^2 L\right)p & +\gamma\frac{V_E}{R}\left(\omega_{ie}\cos L+\frac{V_E}{R}\sec^2 L\right)p
\end{bmatrix}
$$

Fig. 8 Characteristic Matrix of Velocity Coupled Inertial-Doppler Gyrocompass

$$\Delta = p^5 (p^2+\gamma p+K\omega_s^2)\left[p^5+(2\gamma+\frac{GV_E}{R})p^4+\right.$$
$$+(\gamma^2+\omega_{ie}^2+K\omega_s^2+\frac{\gamma GV_E}{R}+K\omega_{ie}\frac{V_E}{R}+\omega_{ie}\frac{V_E}{R}+K\frac{V_E^2}{R^2})p^3+$$
$$+(2\gamma\omega_{ie}^2+3\gamma\omega_{ie}\frac{V_E}{R}+\gamma K\omega_s^2+\gamma(K+1)\frac{V_E^2}{R^2}+\gamma K\omega_{ie}\frac{V_E}{R}-G\omega_s^2\omega_{ie}-KG\omega_s^2\frac{V_E}{R})p^2$$
$$+(\gamma^2\omega_{ie}^2+\omega_s^2\omega_{ie}^2+2\gamma^2\omega_{ie}\frac{V_E}{R}+\gamma^2\frac{V_E^2}{R^2}+(K+1)\omega_s^2\omega_{ie}\frac{V_E}{R}-\gamma\omega_s^2\omega_{ie}G+K\omega_s^2\frac{V_E^2}{R^2})p$$
$$\left.+\gamma\omega_s^2(\omega_{ie}^2+(K+1)\omega_{ie}\frac{V_E}{R}+\frac{KV_E^2}{R^2})\right] = 0$$

From inspection of the coefficient of the $p^4$ term, a necessary but not sufficient condition for stability is that

$$G < \frac{2\gamma R}{|-V_E|_{(MAX)}}$$

At SST speeds, the magnitude of gain G, which determines settling time of the gyrocompass, is severely limited. Cause of the instability is the cross-coupled east velocity term of the north component of resolved doppler velocity. As the angle $C_z$ changes, the magnitude of the cross-coupling term varies, and coupled to the north velocity integrator by gain $\gamma$, is treated as an acceleration input. An equivalent acceleration is not physically present to be sensed by the x-axis accelerometer. At sufficiently high easterly velocity, the offending cross-coupled velocity term, being of opposite sign as the gravitational tilt sensed by the accelerometer, commands the space integrator to diverge from the desired z-axis alignment.

## CHAPTER IV

## RESULTS OF ERROR ANALYSIS

A solution in closed form of equation set (13) was not attempted. With the aid of a digital computer specialized solutions were obtained. Three basic configurations of navigation system were studied. **Referring to Figure (4) and letting** $H_1(p) = \gamma$, $H_2(p) = \alpha$, and $H_3(o) = 0$, the characteristic equation of this isolated single channel is

$$p^2 + \gamma p + (1+\alpha)\frac{g}{R} = 0$$

from which the natural frequency $\omega_n$ is

$$\omega_n = \sqrt{1+\alpha}\sqrt{\frac{g}{R}} = \sqrt{K}\omega_s$$

and the damping factor $\zeta$ is

$$\zeta = \frac{\gamma}{2\sqrt{K}\,\omega_s}$$

The first system configuration studied was a pure inertial, undamped, navigator. The other two systems utilize doppler information for damping. In both of the doppler-damped systems, the gains were chosen so to attain a damping factor of 0.7 in each level axis Schuler loop. The three systems studied are characterized by the following:

System "1" - Pure undamped inertial navigator; $\gamma = 0$, $\alpha = 0$, $\omega_n = \omega_s$, $\zeta = 0$.

System "2" - Doppler damped inertial navigator; $\gamma = 6.25$ radians/hour, $\alpha = 0$, $\omega_n = \omega_s$, $\zeta = 0.7$.

System "3" - Doppler damped and tuned inertial navigator; $\gamma = 31.2$ radians/hour, $\alpha = 24$, $\omega_n = 5\omega_s$, $\zeta = 0.7$

Component uncertainties were assumed to be constant biases. The flight conditions assumed were constant altitude and velocity, taken as a pure east-west velocity of 2000 knots. Both easterly and westerly flight were simulated. These two velocities were chosen to approximate the extremes of space-referenced velocity to be experienced by the advanced SST.

Using a digital computer, matrix equation set (13) was solved for each transfer function from component uncertainty to navigational correction. Inverse Laplace transforms were computed and the time response plotted for six hours of flight. These plots are contained in the appendix.

Taking typical inertial component uncertainties to be on the order of one arc-minute per hour gyro drift and $10^{-4}$ g accelerometer bias, the major cause of navigational error in the pure undamped inertial system (system 1 in the plots) is gyro drift. Both latitude and true heading corrections due to gyro drift are bounded, oscillating with a space rate period of about six hours flying east, or about 12 hours flying west (2000 knots at 45 degrees latitude). Longitude error increases monotonically with time. Some plots also show an 84 minute Schuler modulation imposed on the space rate mode, but the amplitude of the Schuler oscillation is relatively low compared to the space rate mode.

Compared to the pure inertial navigator, the doppler-inertial systems exhibited the following performance:

(i) In all cases the 84 minute Schuler oscillation was suppressed by both systems 2 and 3 .

(ii) System 3 changed both the period and amplitude of the space rate mode of latitude correction from azimuth (z-axis) gyro drift. Period and amplitude were lowered for the easterly flight, raised for the westerly flight. System 2 did not significantly change the latitude correction from azimuth gyro drift.

(iii) System 3 suppressed longitude correction from azimuth gyro drift for both easterly and westerly flight. System 2 had little effect on this transfer function, except suppression of the relatively unimportant Schuler mode.

(iv) System 3 suppressed both latitude and longitude error due to level-axis gyro drift affecting accelerometer tilt in that channel; i. e., latitude error from y-axis gyro drift, longitude error from x-axis gyro drift. In place of level gyro drift caused error, a high sensitivity to doppler error appeared.

(v) System 3 suppressed true heading error due to y-axis gyro drift, but showed a high sensitivity to x-axis doppler error.

(vi) With the gains chosen, damping of the space rate mode by system 3 was negligible. Figure 8 shows latitude correction over a 24 hour run due to x-axis gyro drift. Damping is insignificant at 24 hours.

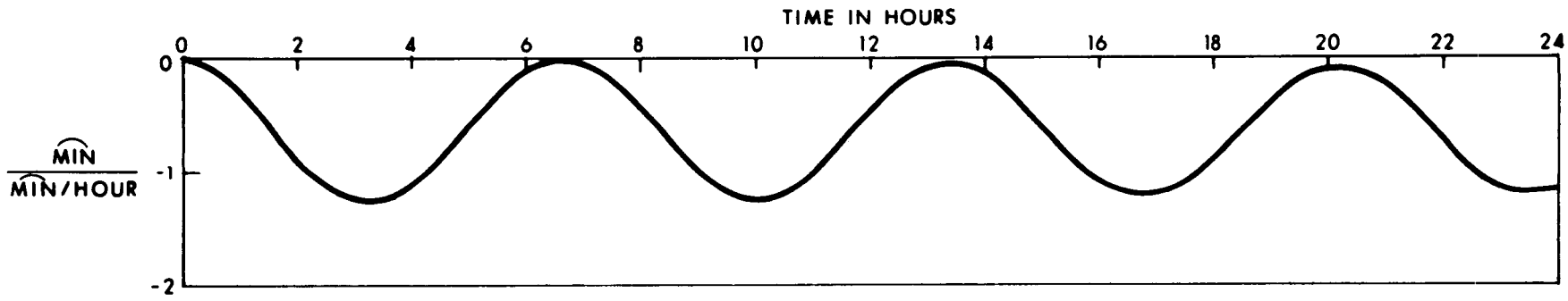


Fig. 8 Latitude Correction Due to Constant X-Axis Gyro Uncertainty, System 3
Easterly Flight at 2000 Knots, 45° North Latitude

In general, wherever sensitivity to either x- or y-axis gyro drift was markedly reduced by system 3, reduced sensitivity to gyro uncertainty was traded for sensitivity to doppler uncertainty. The resulting navigational correction had the same functional form in either case, whether oscillating bounded at the space rate period or increasing monotonically. In effect on navigational performance, one knot of doppler bias uncertainty is approximately equivalent to one arc-minute per hour of level axis gyro drift.

# CHAPTER V

## CONCLUSIONS

It was found that the dominant error mode for SST inertial navigator operation is a bounded oscillation at the space rate period in latitude and true heading, and is unbounded in longitude (system 1). Doppler damping by feedback around the velocity integrator (system 2) does not significantly reduce the magnitude of these dominant error modes, and thus would be of little utility in the SST application. Further use of doppler information as a feed-forward correction (system 3) substitutes a dependency on doppler bias uncertainty for level-axis gyro drift, with one knot of doppler bias being equivalent to one arc-minute per hour of level-axis gyro drift. The requirement for a quality azimuth gyro is important in all three systems.

Bias uncertainty in doppler radar velocity determination is largely proportional to the speed of flight. Typical magnitudes of bias uncertainty are 0.1 to 0.4 percent of actual groundspeed.* At SST speeds, available doppler radars and level-axis gyros would offer similar navigational performance. Thus it appears that little would be gained for the SST application by the added complexity of a doppler-inertial system such as system 3.

In conclusion, neither of the hybrid doppler-inertial navigation systems studied offered performance distinctly superior to a pure undamped inertial navigator at SST speeds. Other combinations of inertial and doppler sensors are of course possible, and should be considered, but care must be shown in applying simplified single-axis models, since at high speeds the dominant error modes do not appear in a single-axis analysis. Doppler fluctuation noise, which was not considered in the preceeding study, would be expected to degrade navigational performance in a hybrid system, and should be considered in further studies.

---

* The AN/APN-153(V) used extensively in U. S. Navy aircraft, and the doppler radar under development for the C-5A aircraft are two doppler sensors for which performance specifications are available. The above figures are based on the manufacturer's specifications.

# APPENDIX

## ERROR CURVES

Navigational Corrections Due to Constant Uncertainties in Inertial Sensors and Resolved Doppler Radar Velocity.

Note: All plots at 45 degrees north latitude.

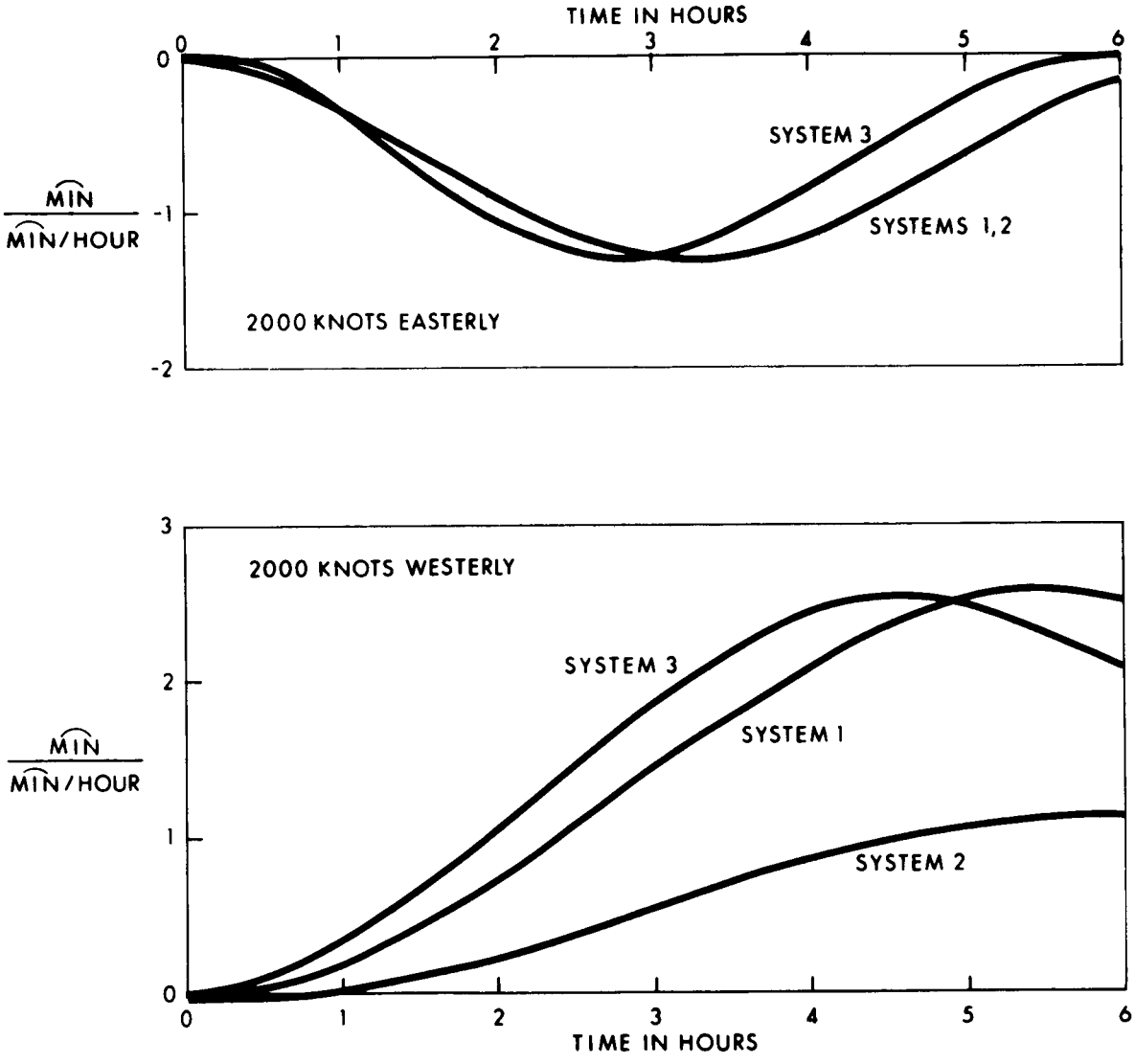


Latitude Correction Due to Constant X-axis Gyro Uncertainty

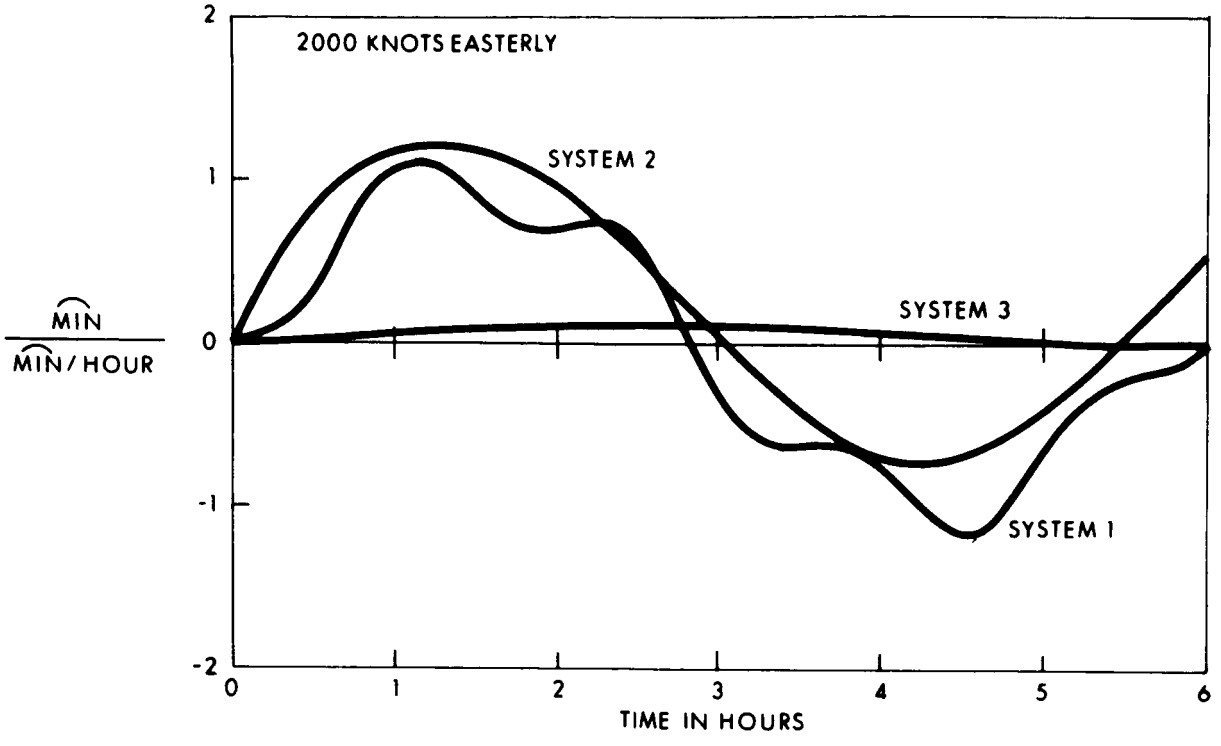


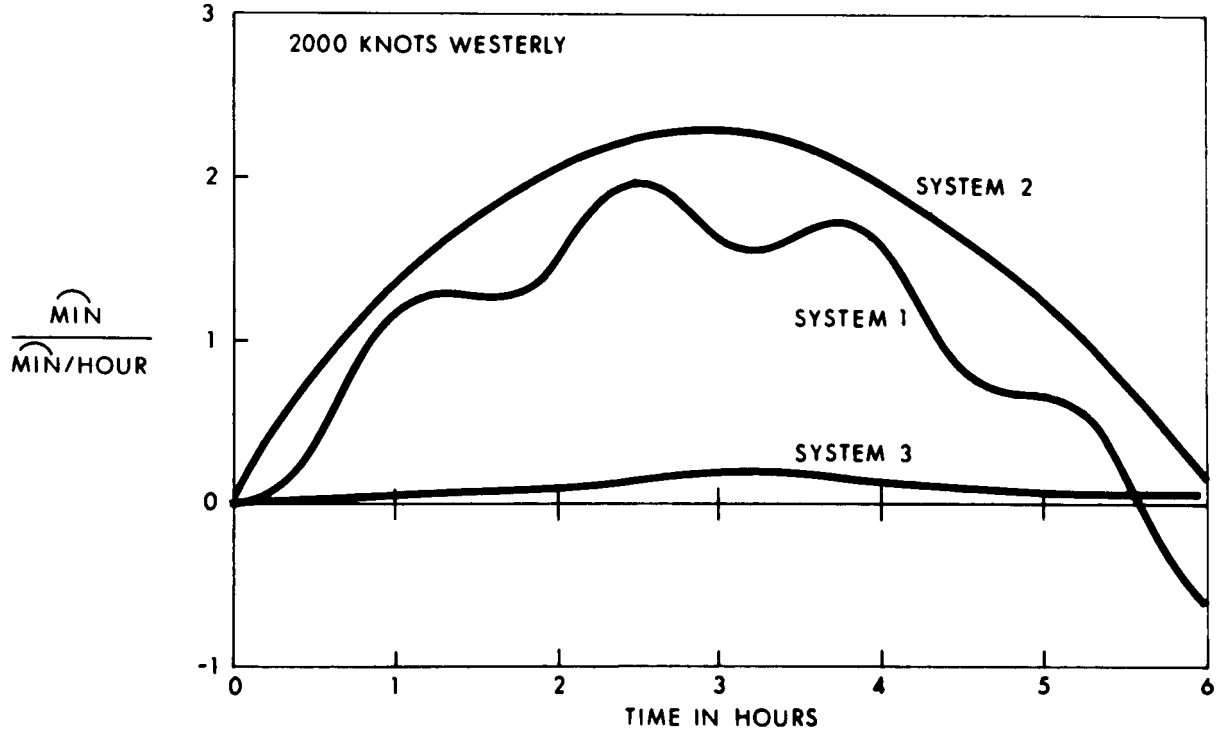


Latitude Correction Due to Constant Y-axis Gyro Uncertainty

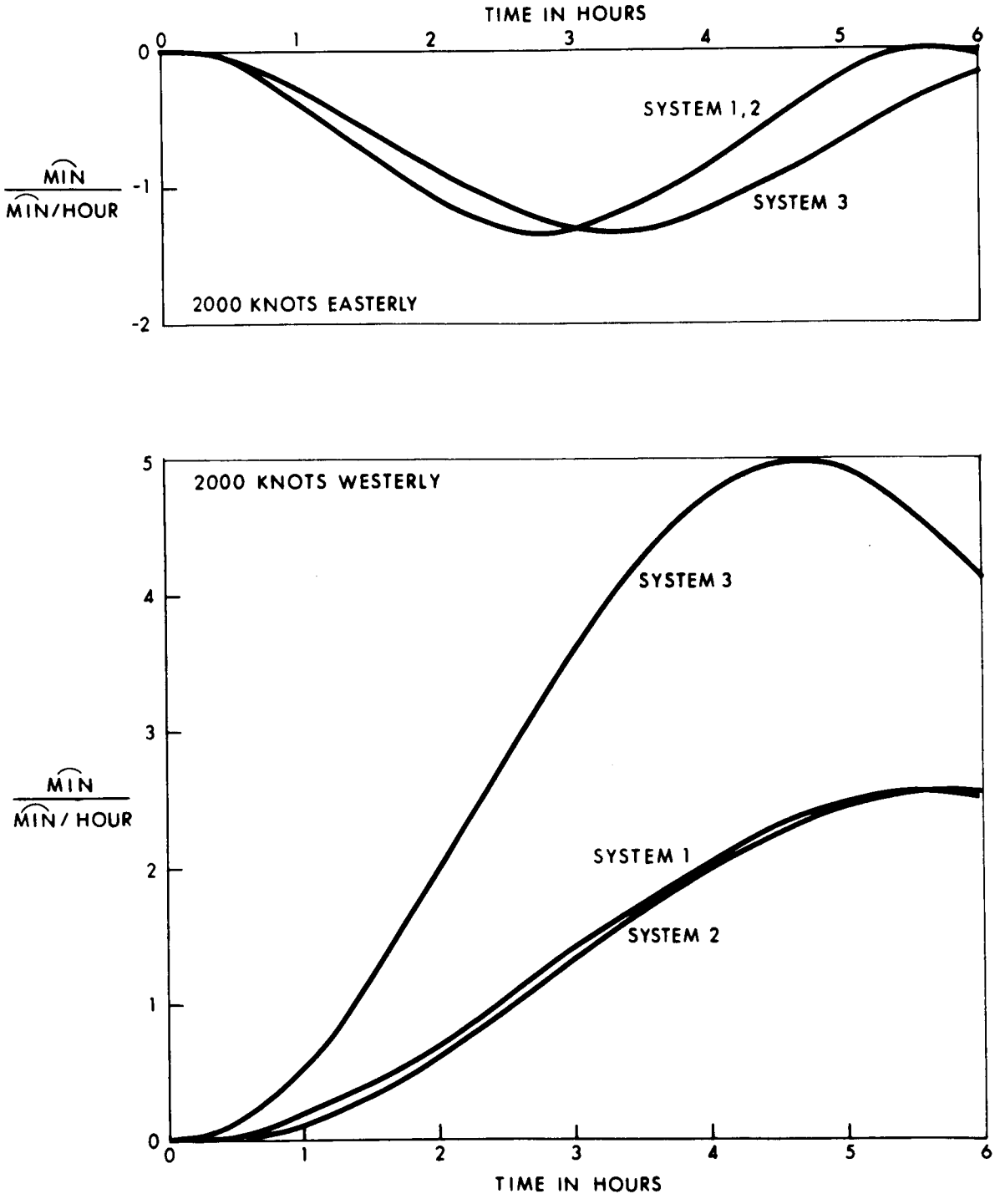


Latitude Correction Due to Constant Z-axis Gyro Uncertainty

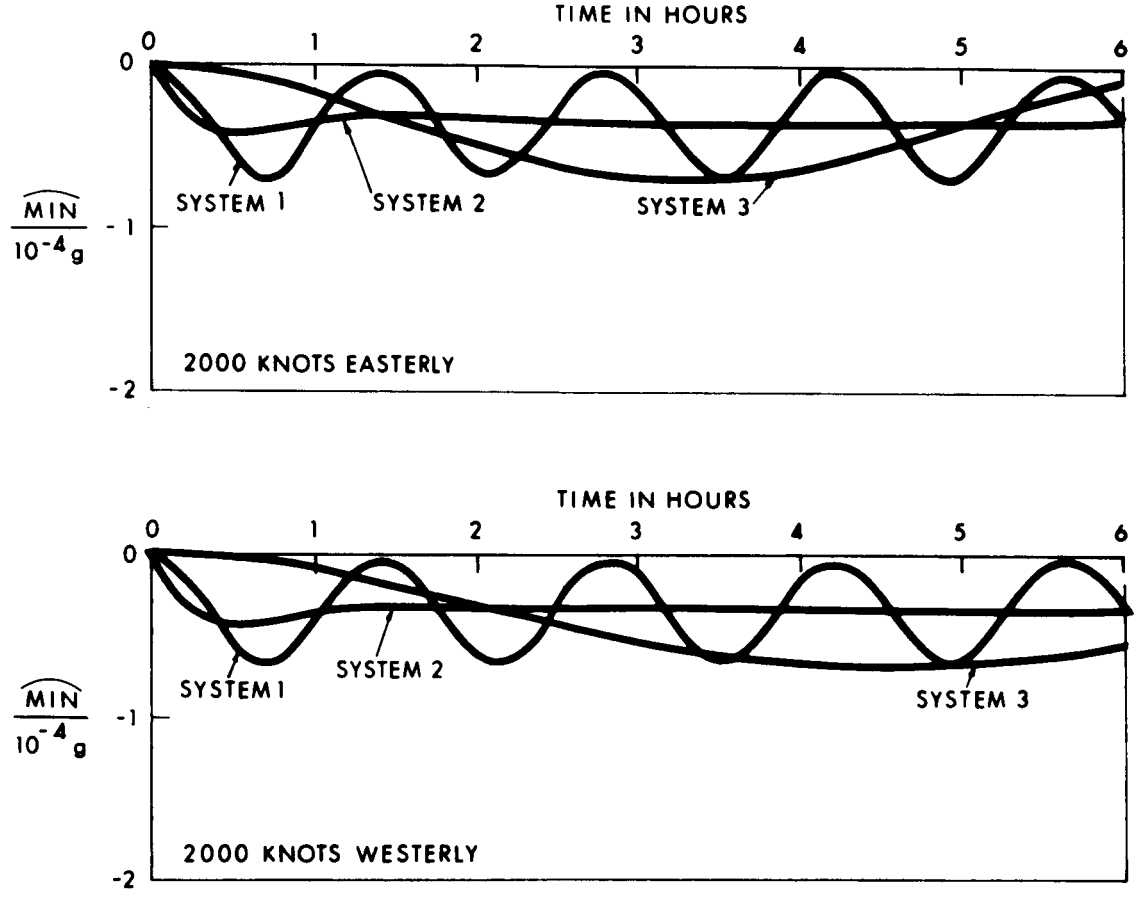


Latitude Correction Due to Constant X-accelerometer Uncertainty

(Note: Zero latitude correction for constant Y-accelerometer uncertainty.)

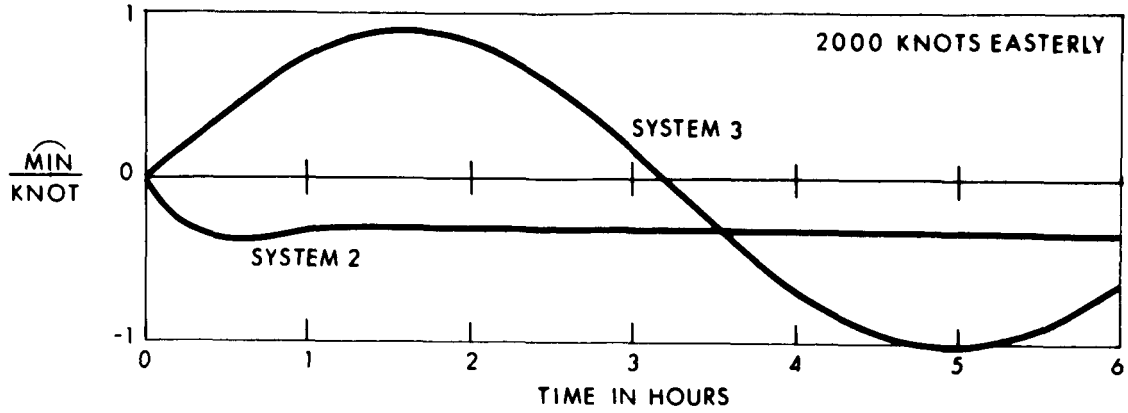


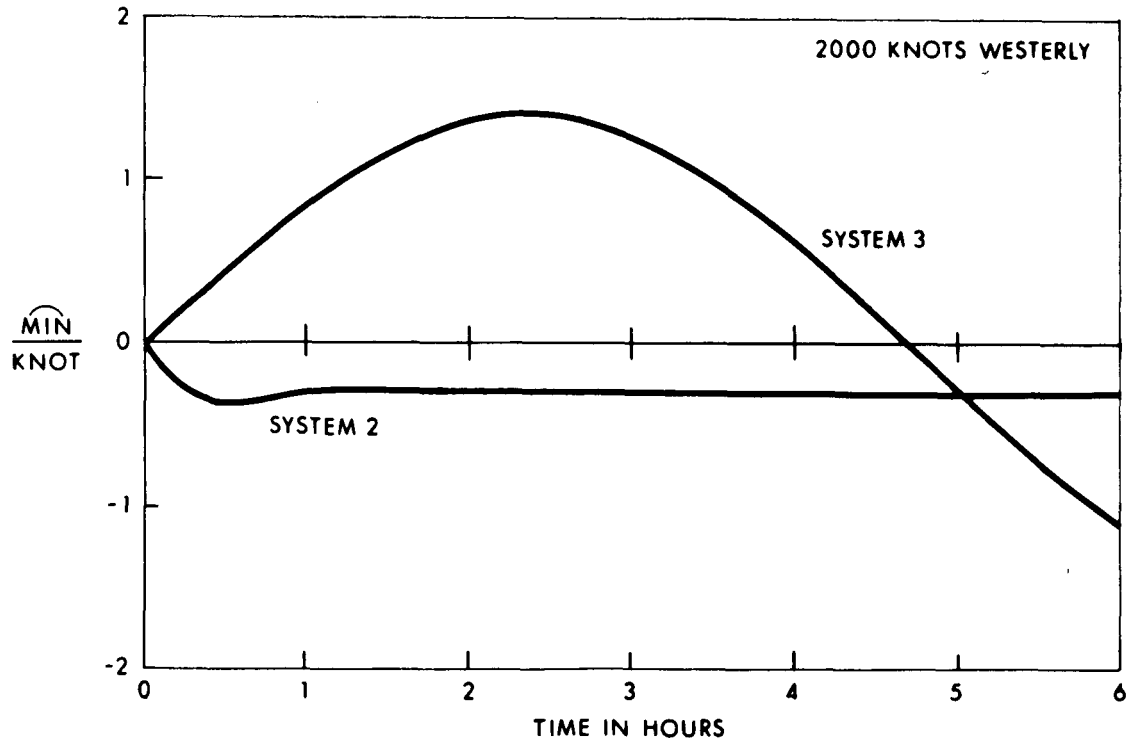


Latitude Correction Due to Constant Uncertainty in X-axis Component of Resolved Doppler Velocity

(Note: Zero latitude correction due to constant uncertainty in Y-axis component of resolved doppler velocity.)

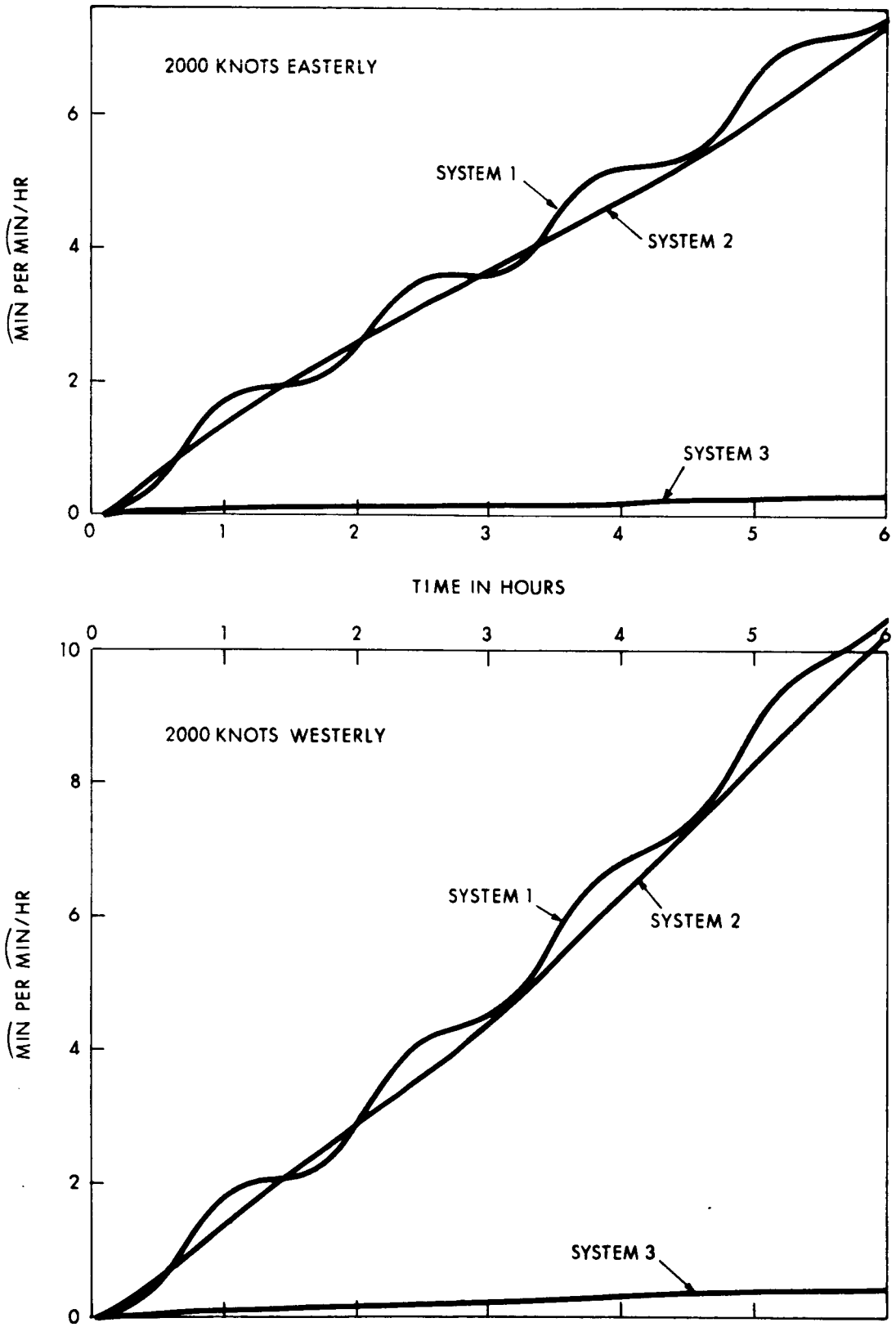


Longitude Correction Due to Constant X-axis Gyro Uncertainty

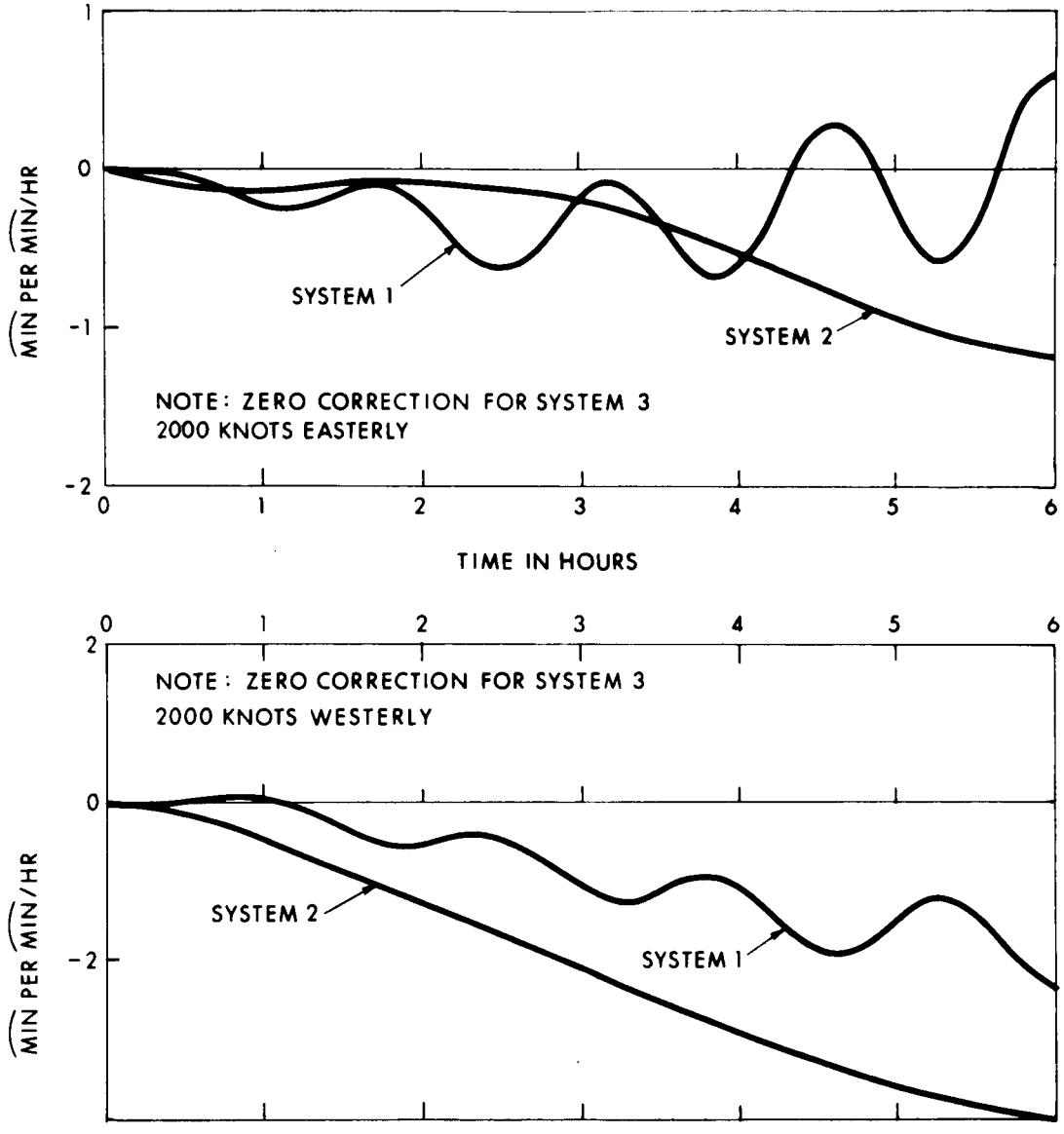


Longitude Correction Due to Constant Y-axis Gyro Uncertainty

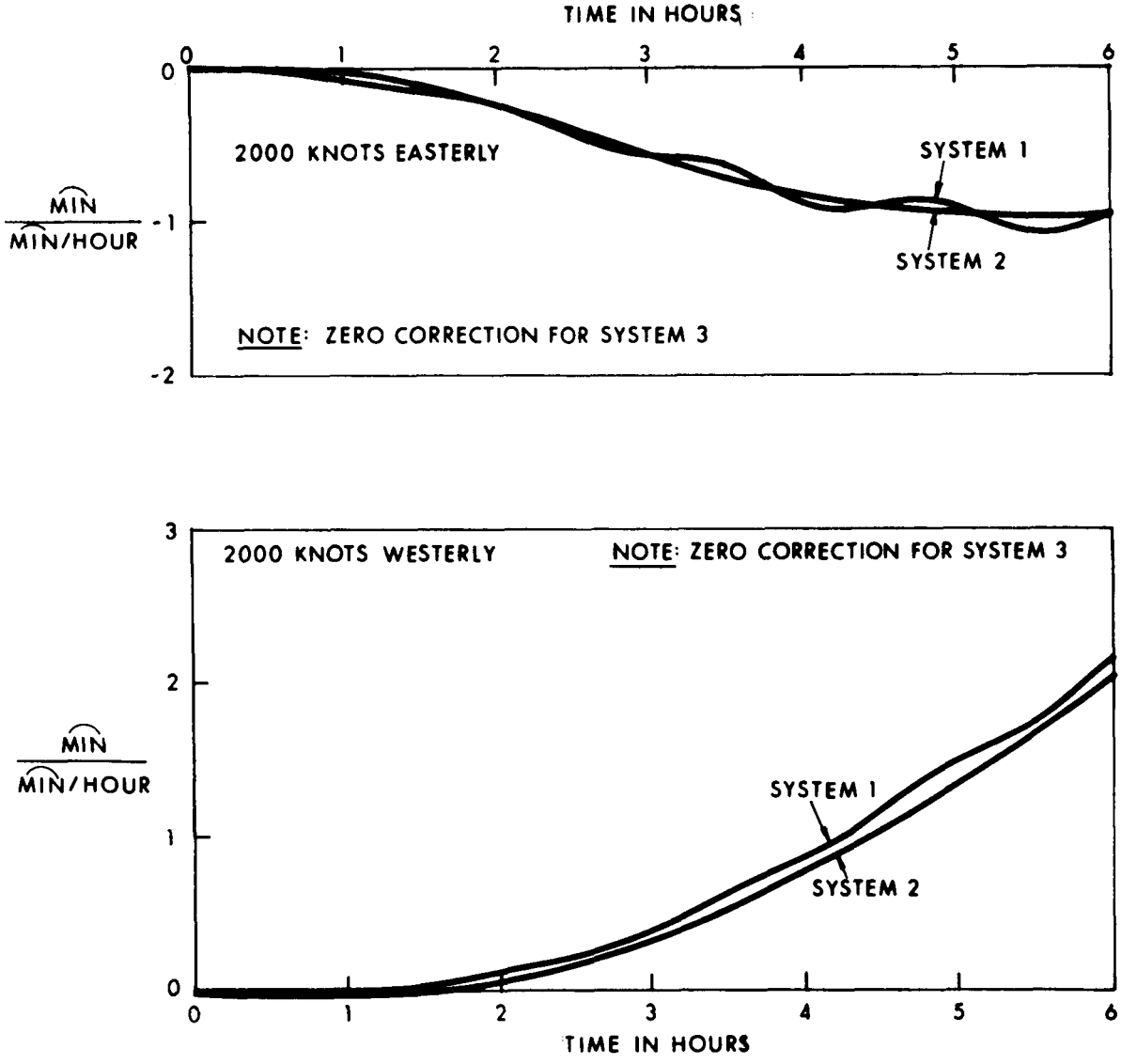


Longitude Correction Due to Constant Z-axis Gyro Uncertainty

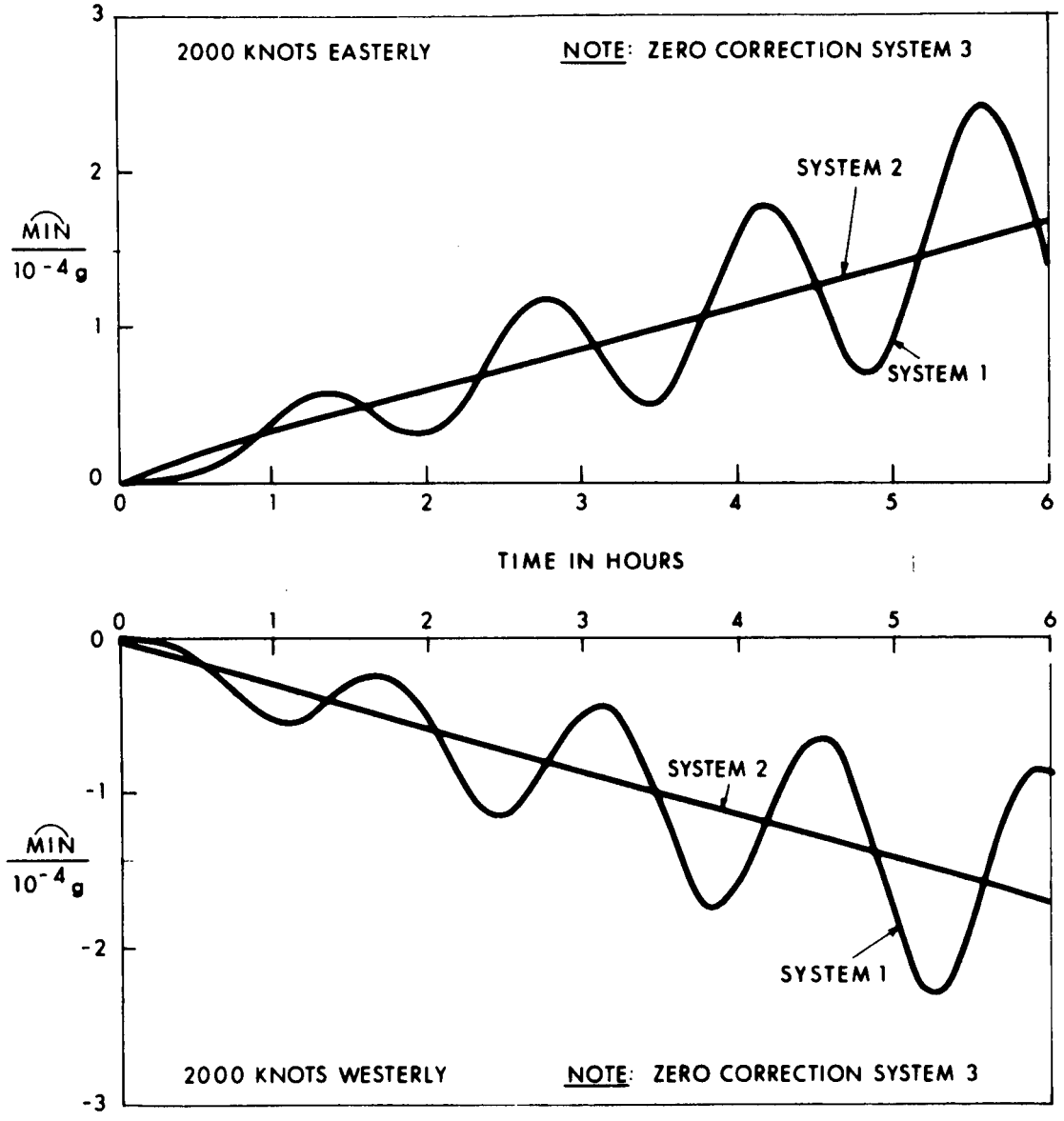


Longitude Correction Due to Constant X-accelerometer Uncertainty

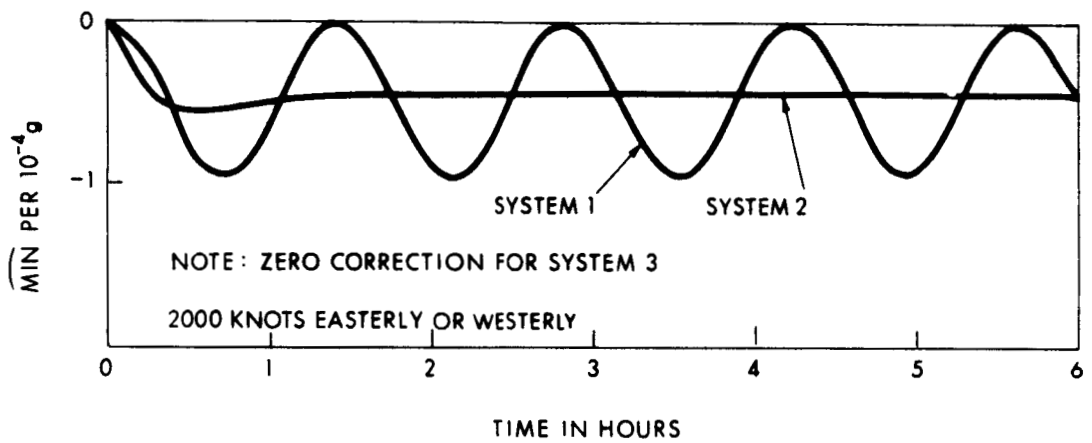


Longitude Correction Due to Constant Y-accelerometer Uncertainty

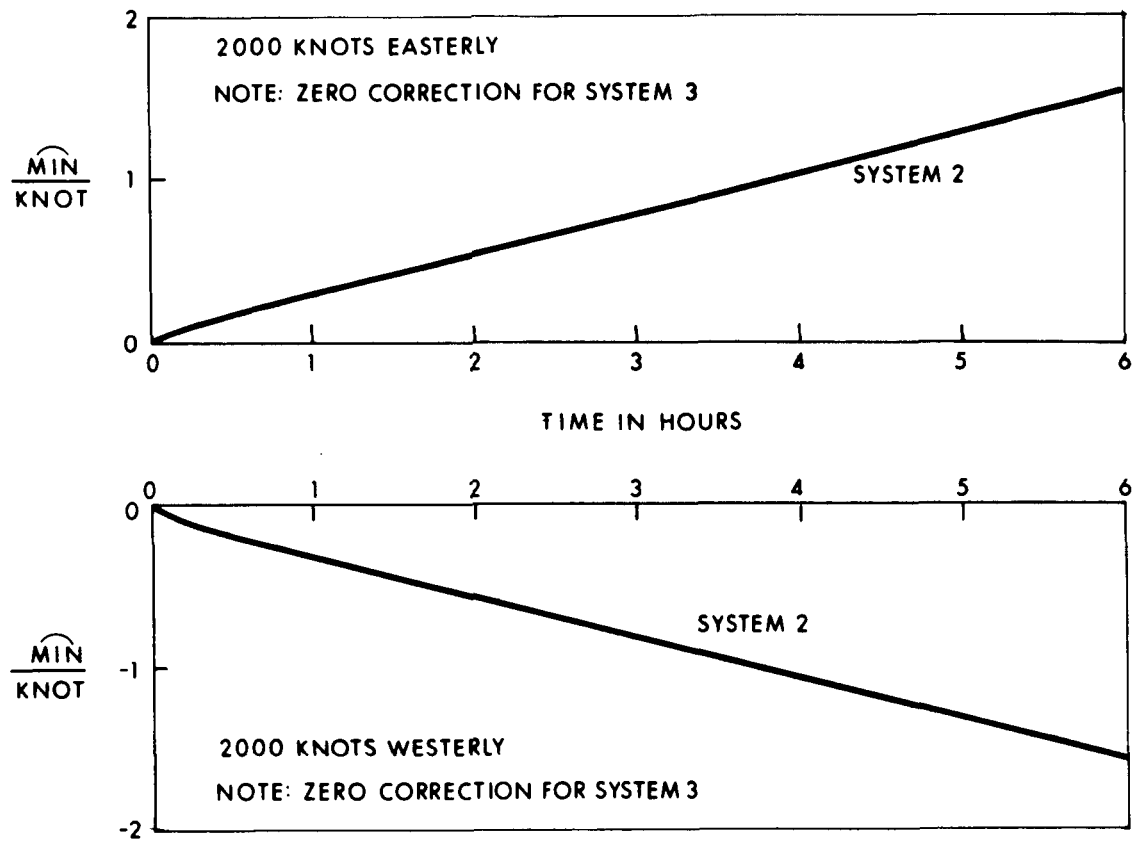


Longitude Correction Due to Constant Uncertainty in X-axis Component of Resolved Doppler Velocity

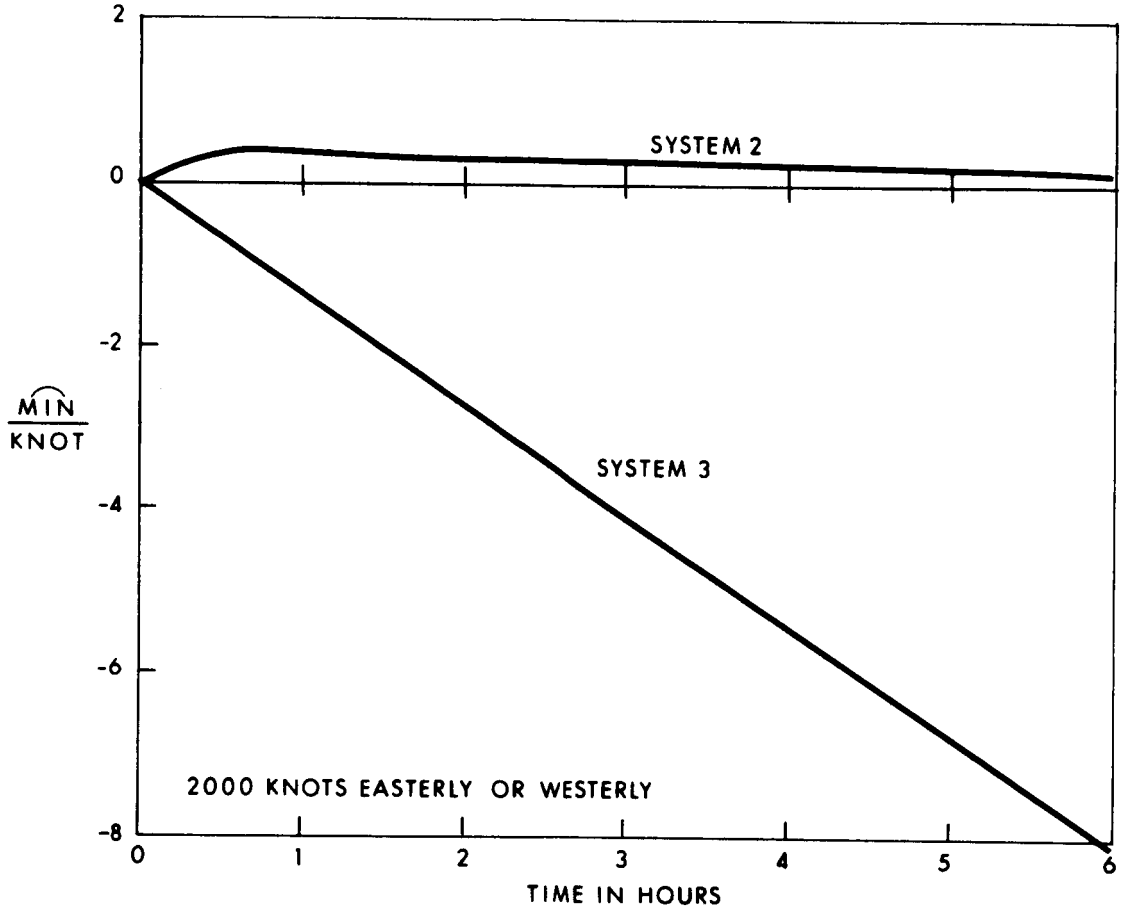


Longitude Correction Due to Constant Uncertainty in Y-axis Component of Resolved Doppler Velocity

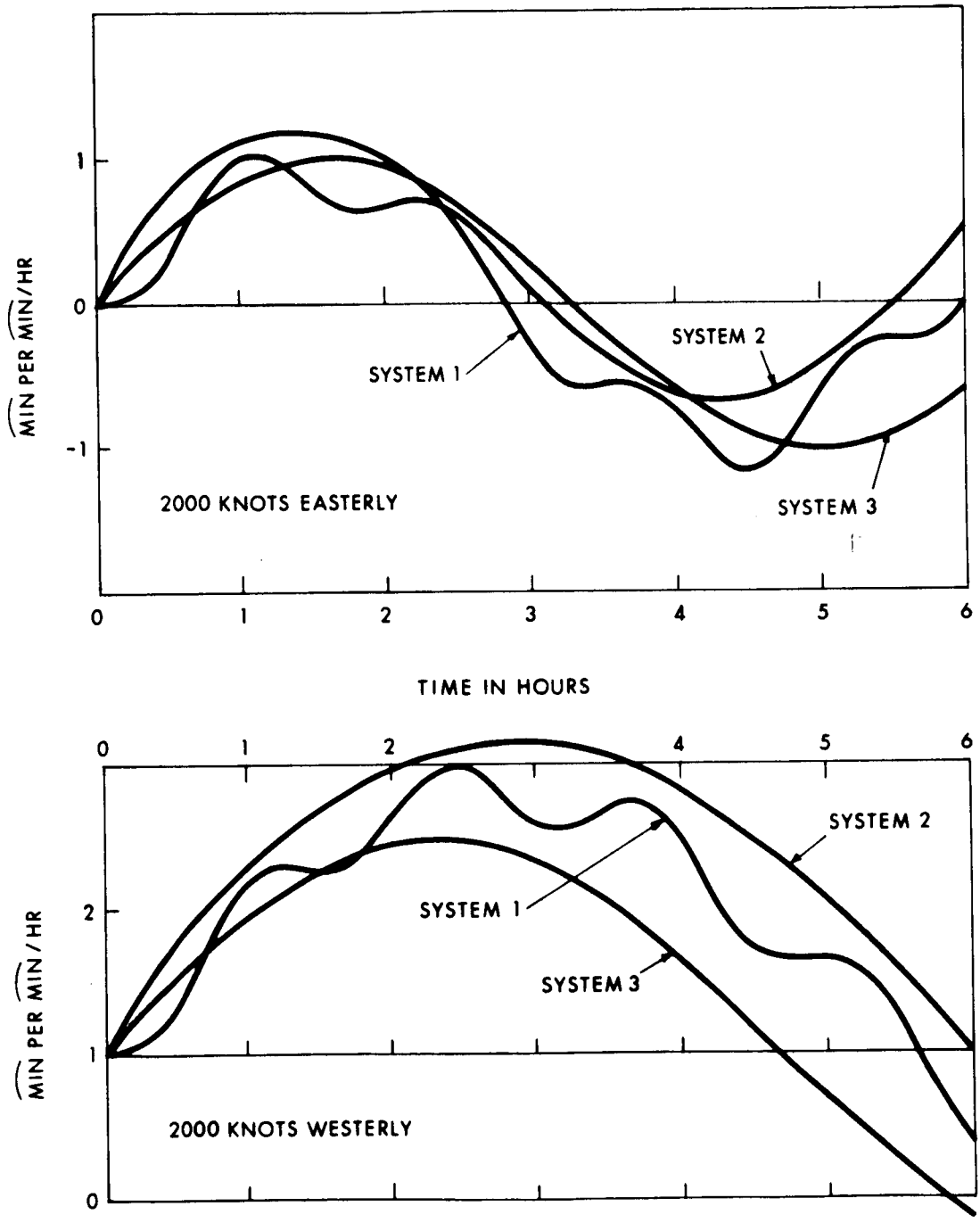


True Heading Correction Due to Constant X-axis Gyro Uncertainty

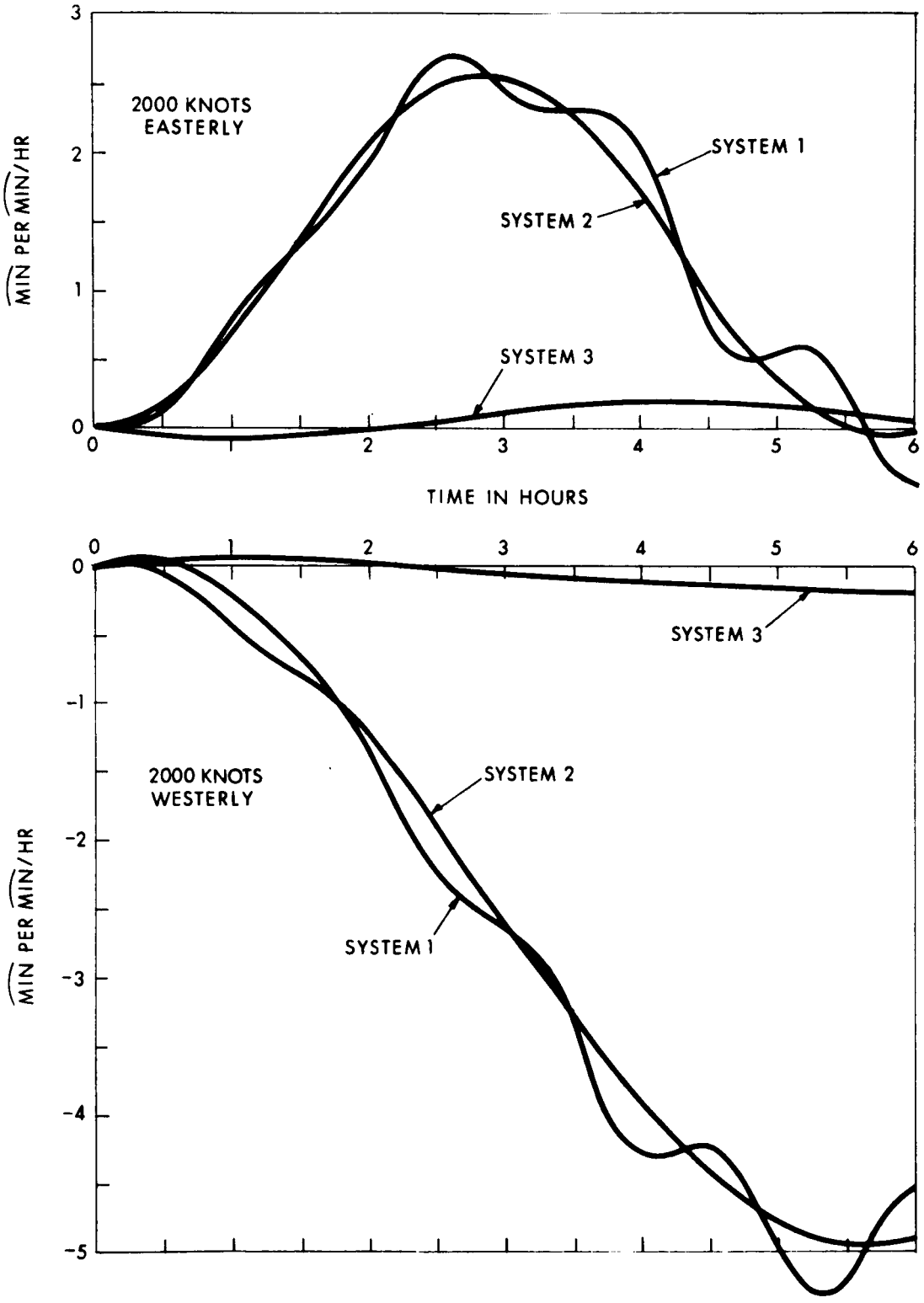


True Heading Correction Due to Constant Y-axis Gyro Uncertainty

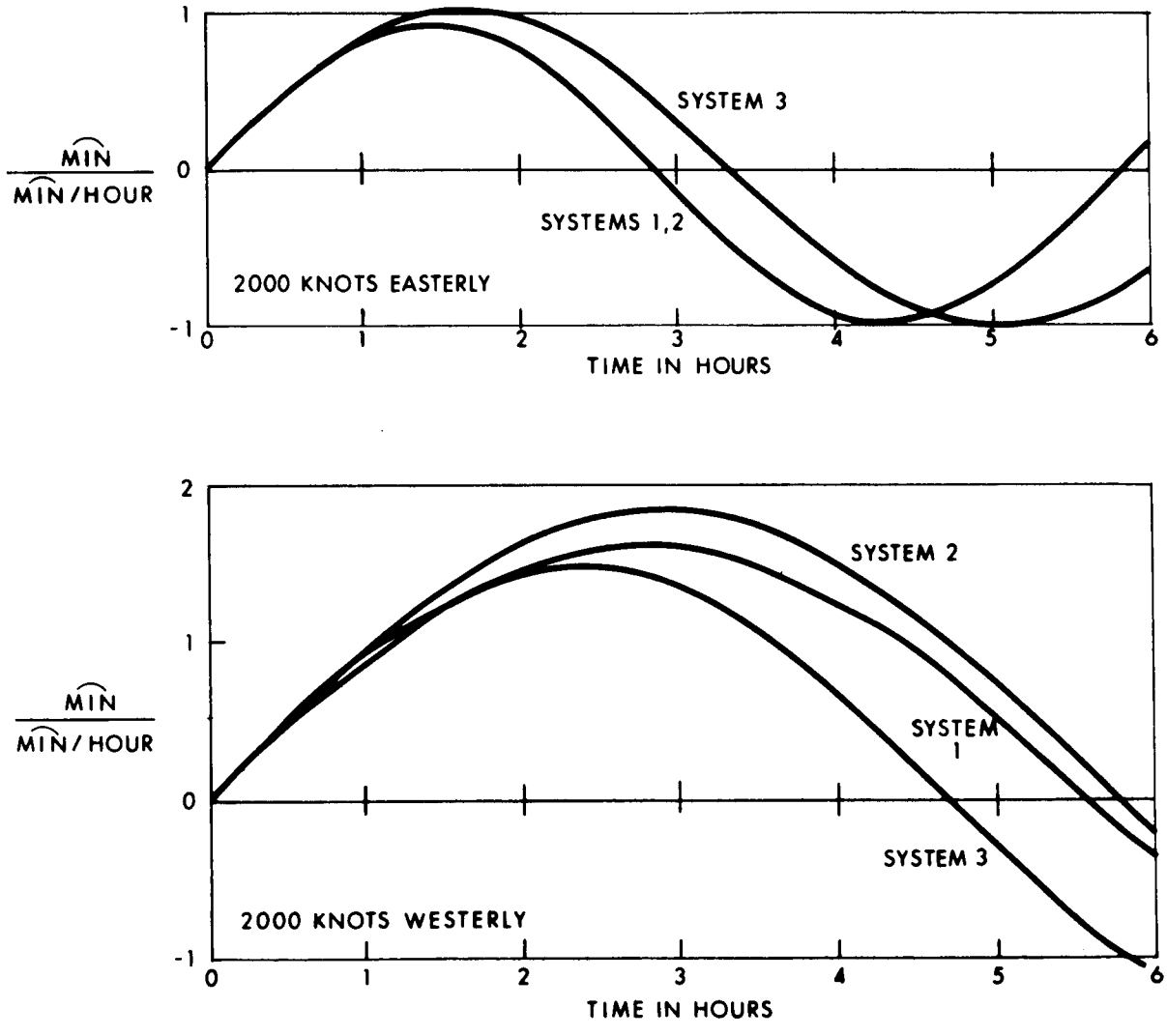


True Heading Correction Due to Constant Z-axis Gyro Uncertainty

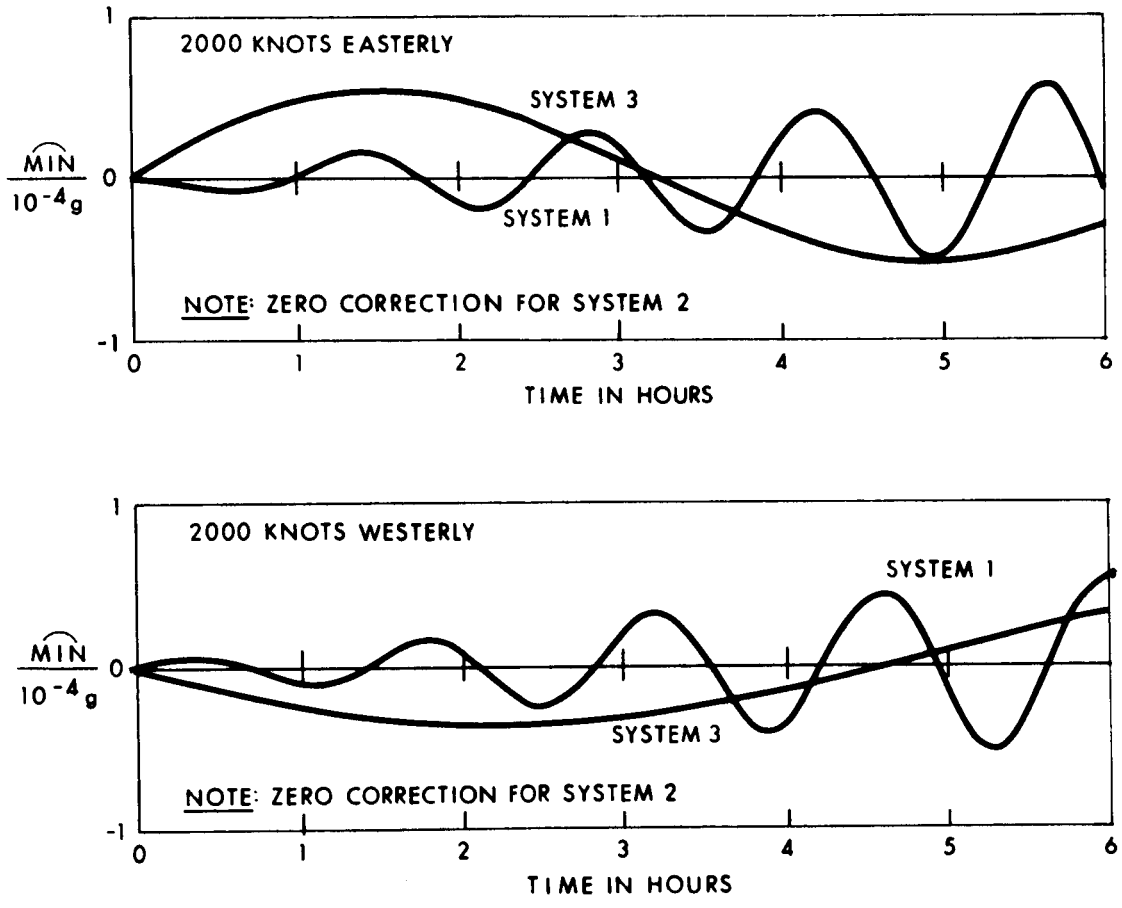


True Heading Correction Due to Constant X-accelerometer Uncertainty

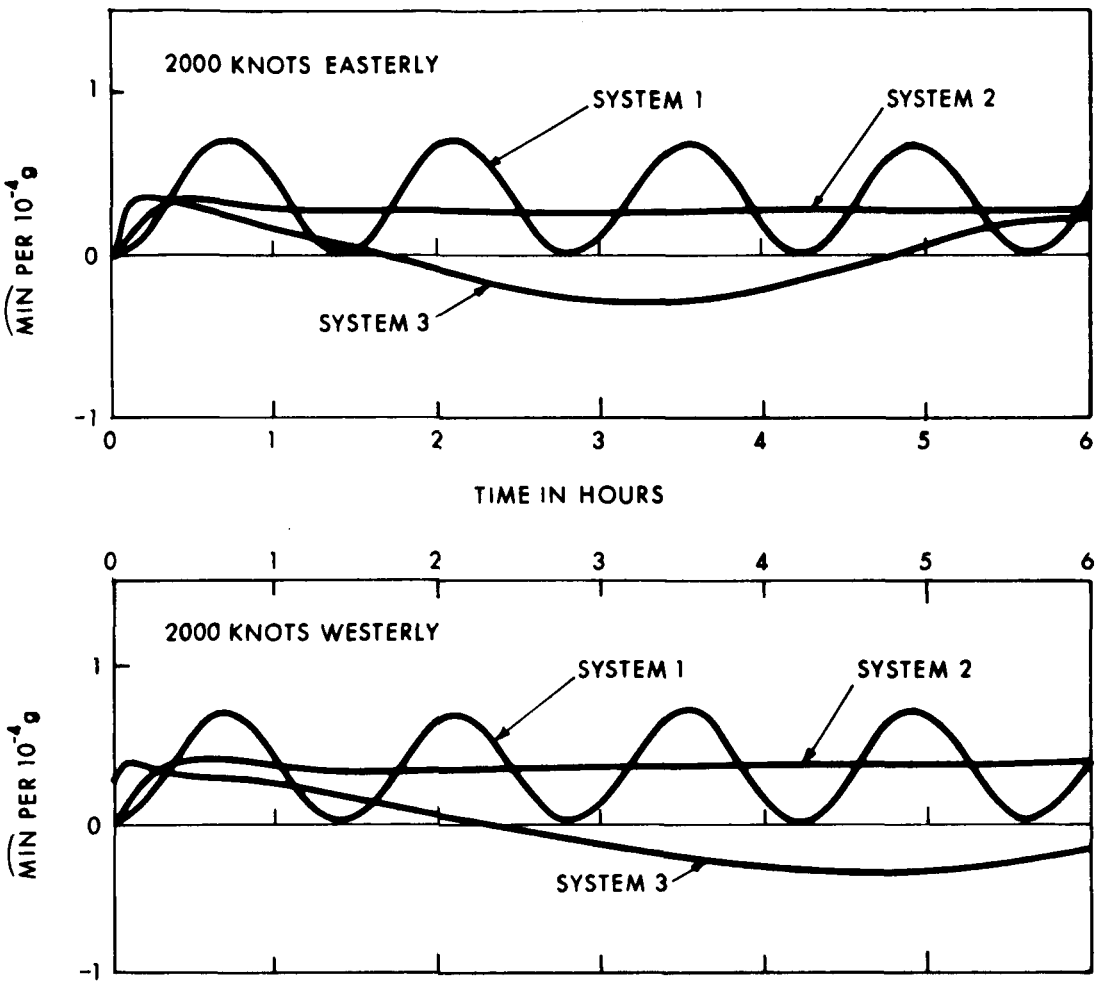


True Heading Correction Due to Constant Y-accelerometer Uncertainty

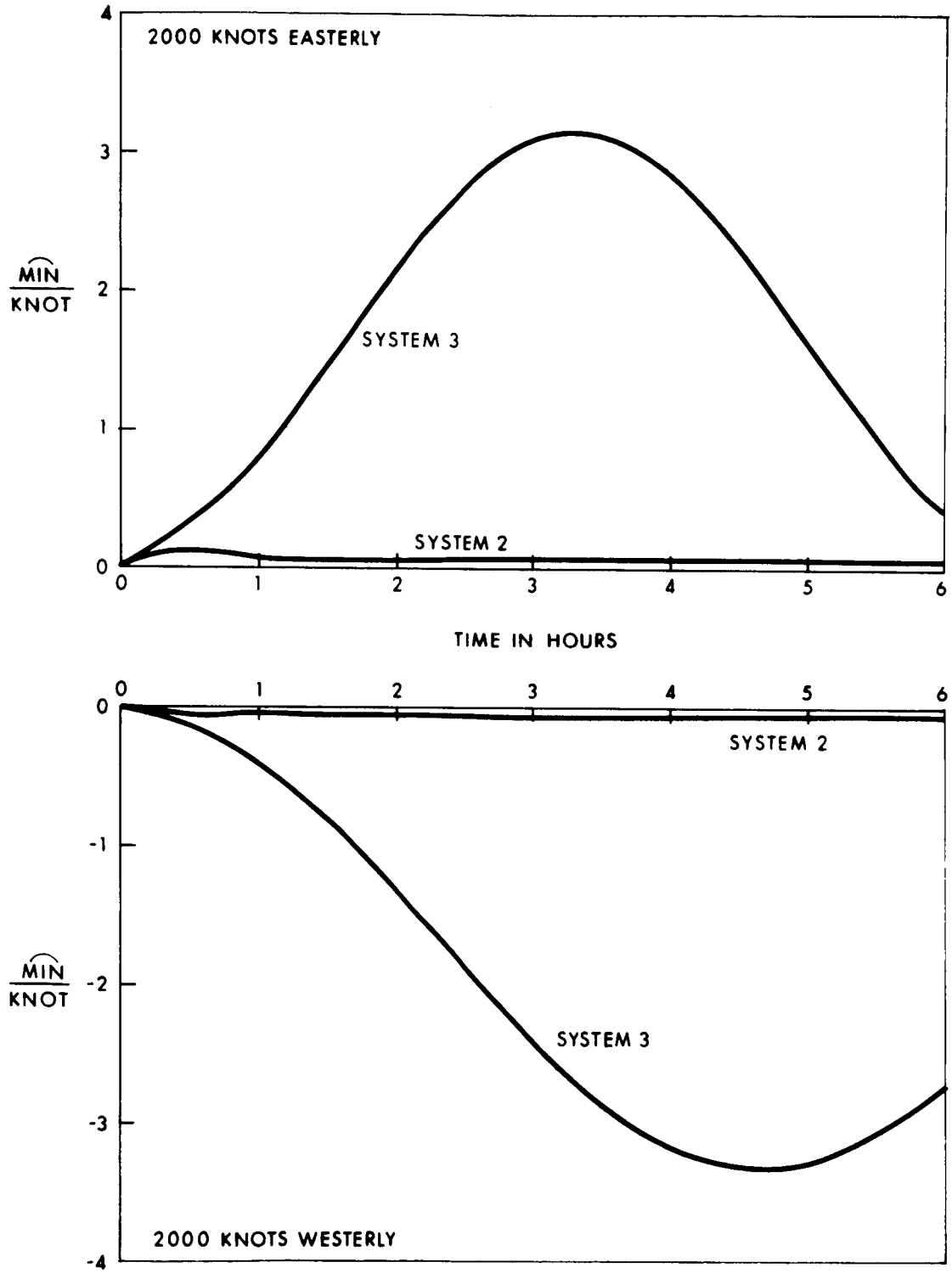


True Heading Correction Due to Constant Uncertainty in X-axis Component of Resolved Doppler Velocity

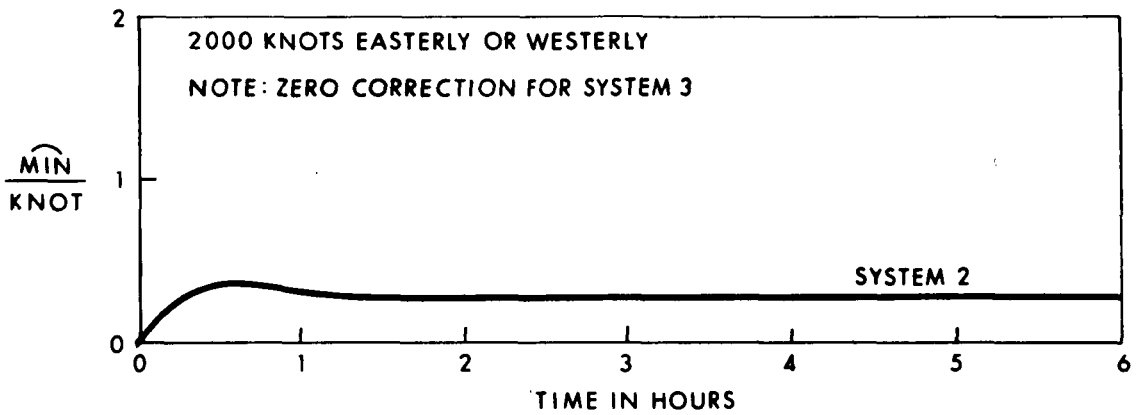


True Heading Correction Due to Constant Uncertainty in Y-axis Component of Resolved Doppler Velocity

## REFERENCES


(1) Fleischmann, L., "A Generalized Formula for the Doppler Effect," Journal, Optical Society of America, Vol. 29, July 1939, pp. 302-304.

(2) Dworetzky, L. H., and Edwards, A., "Principles of Doppler-Inertial Guidance," Journal, American Rocket Society, Vol. 29, No. 12, Dec. 1959, pp. 967-972.

(3) Buell, H., "Doppler, Inertial and Doppler-Inertial Techniques," Navigation, Vol. 11, No. 3, Autumn 1964, pp. 250-259.

(4) Duncan, D. B., "Combined Doppler Radar and Inertial Navigation Systems," Navigation, Vol. 6, No. 5, Spring 1959, pp. 321-327.

(5) Snead, J. C., An Investigation of Noise and Bias Effects on Doppler-Inertial Navigation System Accuracy, M. S. Thesis, June 1965, Air Force Institute of Technology, Wright-Patterson Air Force Base, Ohio, School of Engineering.

(6) Porter, W. A., "Composite Navigation Systems: Current Progress and Potential," Navigation, Vol. 10, No. 2, Summer 1963, pp. 176-182.

(7) Broxmeyer, C., Inertial Navigation Systems, p. 147, McGraw-Hill, New York, N. Y., 1964.

(8) Britting, K. R., Effect of Torquing Uncertainty on Navigation Errors for Local-Vertical and Space-Stabilized Navigation Systems, p. 27, Instrumentation Laboratory, Massachusetts Institute of Technology, Cambridge, Mass., Report E-1946, Jan. 1966.

(9) Markey, W. R., and Hovorka, J., The Mechanics of Inertial Position and Heading Indication, p. 42, Methuen, London, 1961.

(10) Mason, S. J., "Feedback Theory - Further Properties of Signal Flow Graphs," Proceedings, IRE, Vol. 44, No. 7, July 1956, pp. 920-926.

(11) Kaplan, W., Operational Methods for Linear Systems, p. 406, Addison-Wesley, Reading, Mass., 1962.